이학박사 학위논문

장내 뮤신 분해균인 *Akkermansia muciniphila*가 상피 세포의 발달에 미치는 영향과 기전

Effect and mechanism of gut mucin-degrading *Akkermansia muciniphila* on the development of epithelial cells

울산대학교 대학원

의 과 학 과

김 승 일

Effect and mechanism of gut mucin-degrading *Akkermansia muciniphila* on the development of epithelial cells

지 도 교 수 권 미 나

이 논문을 이학박사학위 논문으로 제출함

2021 년 8 월

울산대학교 대학원
의 과 학 과
김 승 일

김승일의 이학박사학위 논문을 인준함

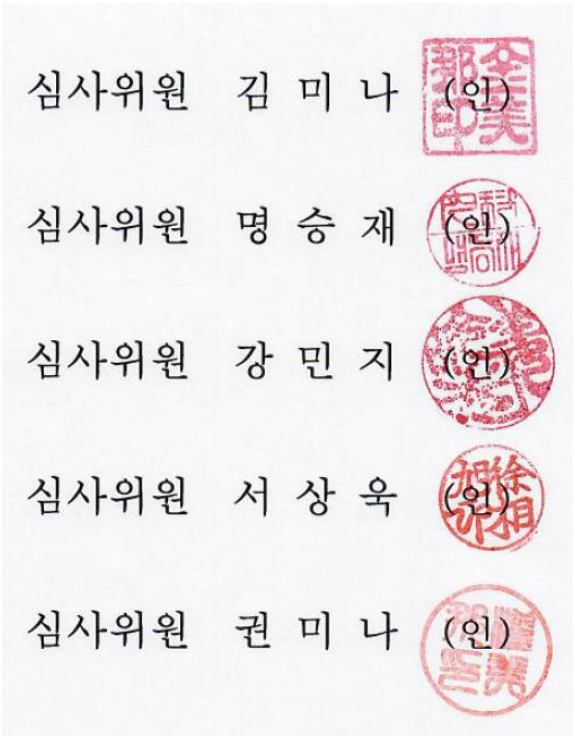

울 산 대 학 교　　대 학 원

2021 년 8 월

Abstract

Mucin-degrading bacteria are densely populated in the intestinal epithelium; however, their interaction with intestinal stem cells (ISCs) and their progeny have not been elucidated. To determine whether mucin-degrading bacteria play a role in gut homeostasis, mice were treated with *Akkermansia muciniphila*, a specialized species that degrades mucin. Administration of *A. muciniphila* for 4 weeks accelerated the proliferation of $Lgr5^{+}$ ISCs and promoted the differentiation of Paneth cells and goblet cells in the small intestine (SI). I found similar effects of *A. muciniphila* in the colon. The levels of acetic and propionic acids were higher in the cecal contents of *A. muciniphila*-treated mice than in PBS-treated mice. SI organoids treated with cecal contents obtained from *A. muciniphila*-treated mice were larger and could be diminished by treatment with G protein-coupled receptor (Gpr) 41/43 antagonists. Pre-treatment of mice with *A. muciniphila* reduced gut damage caused by radiation and methotrexate. Further, a novel isotype of the *A. muciniphila* strain was isolated from heathy human feces that showed enhanced function in intestinal epithelial regeneration. These findings suggest that mucin-degrading bacteria (e.g., *A. muciniphila*) may play a crucial role in promoting ISC-mediated epithelial development and contribute to intestinal homeostasis maintenance.

Keywords: Gut microbiota; *Akkermansia muciniphila*; Intestinal stem cells; Epithelial development

Contents

List of Figures

List of Tables

Introduction

1. Development of intestinal epithelial cells

Control of proliferation and differentiation of intestinal epithelial cells (IECs) is one of the most important factors for maintaining intestinal homeostasis. Mammalian IECs have a rapid turnover rate and are replenished every 3–5 days (Barker, 2014; Clevers, 2013). All types of IECs derive from intestinal stem cells (ISCs) that can generate either ISC daughters or proliferating progenitors called transit-amplifying (TA) cells (Figure 1) (Barker et al., 2007; Bjerknes and Cheng, 1999). TA cells terminally differentiate to secretory lineage cells (e.g., antimicrobial peptide producing Paneth cells, hormone producing enteroendocrine cells, and mucin secreting goblet cells) and absorptive lineage cells (e.g., nutrients absorbing and transporting enterocytes) (Clevers, 2013). As these terminally differentiated cells except Paneth cell reach the tip of villus, they undergo apoptosis and expulsion. Importantly, Paneth cells migrate down into the intestinal crypt bottom to produce ISC niche factors such as Wnt3, EGF, TGF-α, and Dll4 (Sato et al., 2011b) .

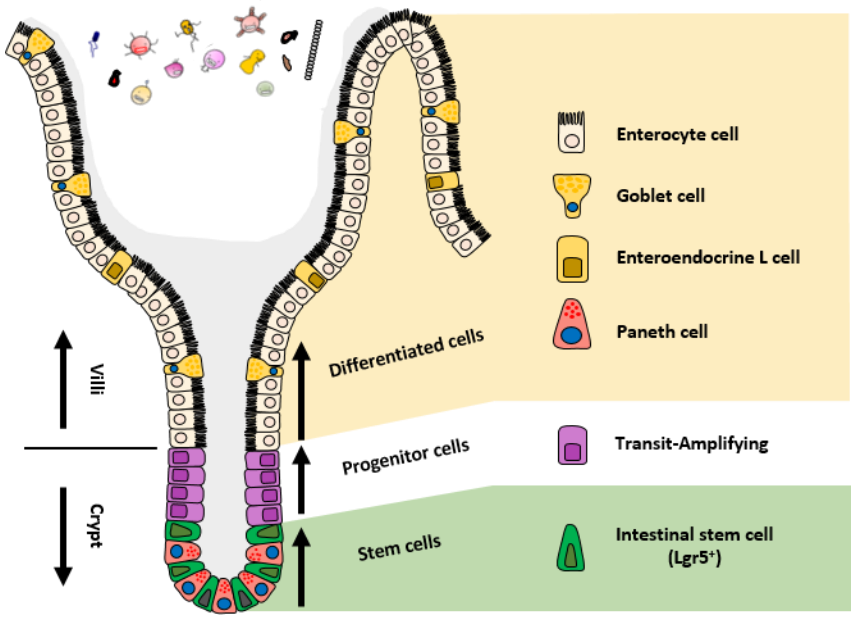

Figure 1. IECs development. Lgr5^{+} ISCs generate transit-amplifying cells, which differentiate into various functional cells on the crypts and villi (Paneth cells, enteroendocrine cells, goblet cells, and enterocyte cells).

2. Wnt signaling in ISCs

The Wnt signaling pathway plays an important role in promoting and driving the proliferative activity of ISCs and IEC differentiation (Korinek et al., 1998; Pinto et al., 2003). A recent study revealed that Wnt/β-catenin signaling supports gut homeostasis by maintaining self-renewal of Lgr5-expressing stem cells in the intestinal crypts (Figure 2) (Farin et al., 2012). The Wnt ligand released from Paneth cells binds to the Frizzled and low-density lipoprotein receptor-related protein receptor. This leads to accumulation of β-catenin, the main mediator of the Wnt signal cascade in the gut (Ireland et al., 2004), which translocates from the cytoplasm into the nucleus. Then, β-catenin binds with the transcription factor, TCF, to regulate the expression of genes involved in proliferation (Behrens et al., 1996; van de Wetering et al., 2002). Without Wnt ligand, the destruction complex (e.g., APC, CK1, GSK3, and Axin) sequentially phosphorylate β-catenin. Phosphorylated β-catenin is target for proteasomal degradation.

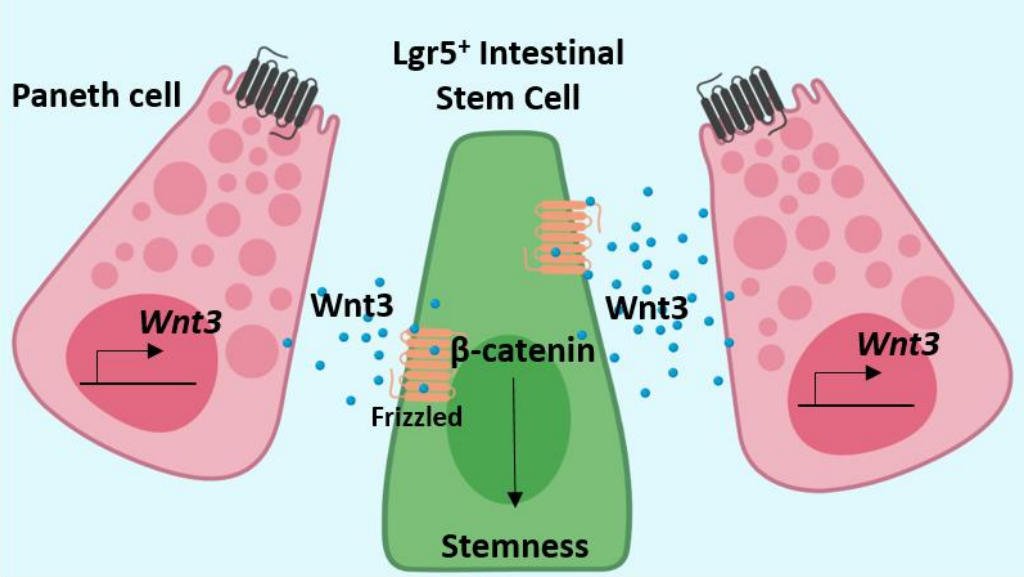

Figure 2. Wnt signaling of IECs. Wnt signaling plays a critical role in IECs development by maintaining stem cell fate. Wnt ligands engage Frizzled receptor, which induce stabilization of β-catenin. β-catenin activates TCF, transcription factors, that support ISCs stemness.

3. Gut microbiota

Our intestine is the harbor of 10^{14} microbiota that mainly consist of bacteria (Xu and Gordon, 2003). Main phylum in the intestine is Firmicutes, Bacteroides, Preteobacteria, Actinobacteria, and Verrucomicrobia (Human Microbiome Project, 2012). Microbiota continually interact with host and contribute to maintain gut homeostasis and host physiology. (Belkaid and Hand, 2014; Skelly et al., 2019). Several studies have identified a link between dysbiosis and disease, such as inflammatory disorder, metabolic syndrome, and central nervous system related illness (Figure 3) (Mazmanian et al., 2008; Turnbaugh et al., 2006; Valles-Colomer et al., 2019).

Metabolites produced by gut microbiota are proposed to modulate host physiology (Furusawa et al., 2013; Koeth et al., 2013; Mazmanian et al., 2008). Short-chain fatty acids (SCFAs; e.g., acetic, propionic, butyric acids) are functional metabolites produced by bacterial fermentation of undigested complex carbohydrates (Miller and Wolin, 1996). By binding to G protein-coupled receptors (Gpr) 41 and 43, SCFAs can affect host gut immunity and metabolism (Figure 4) (Macia et al., 2015; Maslowski et al., 2009). In addition, my group recently suggested that gut microbiota-derived lactate promotes IEC development in a Gpr81-dependent manner (Lee et al., 2018).

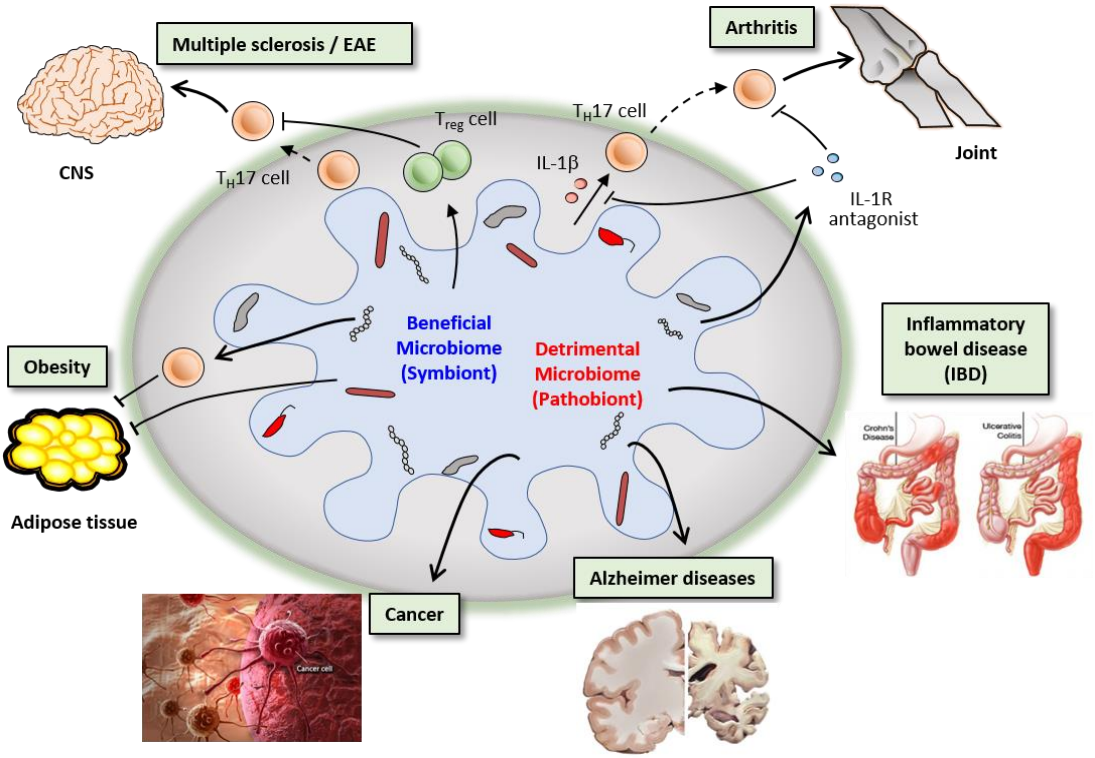

Figure 3. Diseases related to gut microbiota. Microbiota constantly interacts with host. When detrimental microbes are increasing under the dysbiosis condition, pathobiont induces various diseases such as obesity, cancer, inflammatory bowel disease, arthritis, multiple sclerosis, and Alzheimer's diseases.

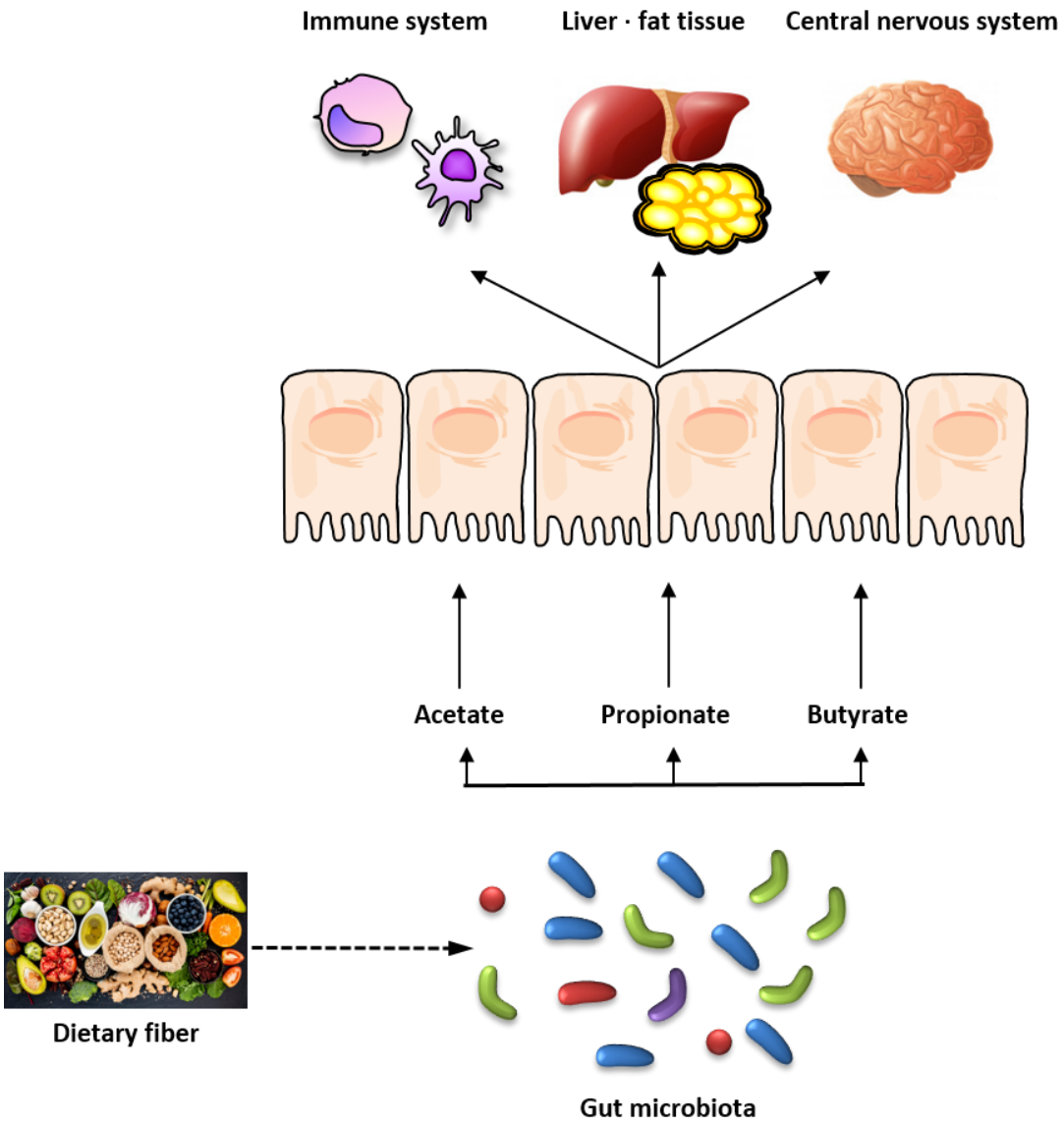

Figure 4. Effect of dietary gut microbial SCFAs on host homeostasis. Fermentation of indigestible polysaccharides such as dietary fiber by gut microbiota produces SCFA (e.g., acetate, propionate, and butyrate), which modulates and affects host physiology.

4. *Akkermansia muciniphila*

Akkermansia muciniphila is a mucin-degrading bacterium and the sole genus of the phylum, Verrucomicrobia, which is found in human stool (Cani and De Vos, 2017). *A. muciniphila* represents approximately 1~3% of intestinal microbiota residing in the mucus layer near the IECs (Derrien et al., 2008; Derrien et al., 2004). Several studies have shown that the abundance of *A. muciniphila* is inversely correlated with various diseases, such as inflammatory bowel disease, diabetes, and obesity (Figure 5) (Alam et al., 2016; Everard et al., 2013; Plovier et al., 2017; Png et al., 2010; Schneeberger et al., 2015). Administration of *A. muciniphila* reduces weight gain and improves metabolic parameters, such as glucose metabolism (Chevalier et al., 2015; Depommier et al., 2019; Everard et al., 2013; Plovier et al., 2017). Metformin, an anti-diabetic agent, increases the abundance of *A. muciniphila* in the gut microbiota of obese mice under diet conditions (Lee and Ko, 2014; Shin et al., 2014). A recent study also demonstrated correlation between the clinical efficacy of immune checkpoint inhibitors and the relative abundance of *A. muciniphila* (Routy et al., 2018). These results indicate that *A. muciniphila* may have potential as a key next-generation microbe with a wide spectrum of therapeutic applications.

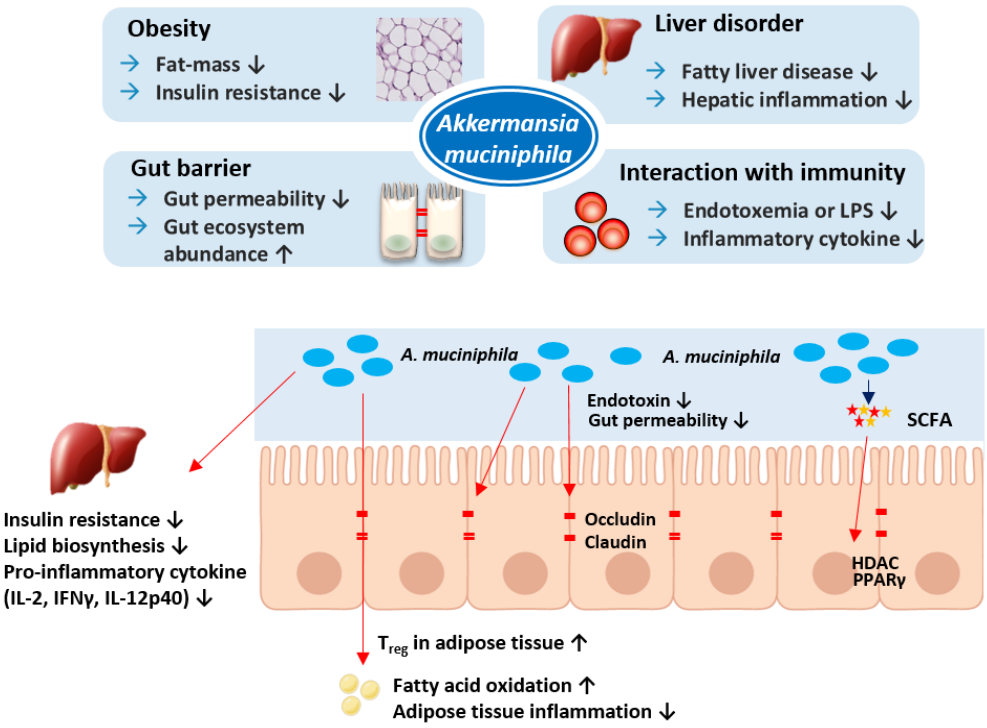

Figure 5. Cross-talk between *A. muciniphila* and host. *A. muciniphila* contributes to maintain host health by preventing metabolic diseases and inflammation, and reinforcing gut barrier.

In this study, I investigated the potential role of *A. muciniphila* in IEC development. I confirmed that despite being a mucin-degrading bacterium, *A. muciniphila* paradoxically increased mucus production by promoting the differentiation of secretory IEC lineages. Administration of *A. muciniphila* enhanced ISC proliferation in a Gpr41/43-dependent manner and subsequently accelerated intestinal epithelial regeneration. Most importantly, *A. muciniphila* protected mice from severe gut damage caused by radiation and chemotherapy. Taken together, my findings suggest that *A. muciniphila* promotes IEC development and maintains gut homeostasis.

Material and Methods

Ethics statement.

All animal experiments were approved by the Institutional Animal Care and Use Committee of Asan Medical Center (Approval No. 2019-12-251). Fecal samples and colon tissues were obtained from the human dock center of the Asan Medical Center under Institutional Review Board (Approval No. A20201614). All experiments were performed under anesthesia with a mixture of ketamine (100 mg/kg) and xylazine (20 mg/kg).

Mice

The mice in this study were 8- to- 10-week-old females that were fed sterile food and water *ad libitum*. C57BL/6 mice were purchased from OrientBio (Seong-Nam, South Korea) and Lgr5-EGFP-IRES-CreERT2 (Lgr5-GFP) mice were purchased from The Jackson Laboratory (Bar Harbor, ME). Mice were housed in the animal facility of the Asan Medical Center (Seoul, South Korea) and maintained under specific pathogen-free conditions. Germ-free mice were maintained in the animal facility at POSTECH (Pohang, South Korea). All experiments were performed in accordance with relevant ethical guidelines and regulations.

Isolation of *A. muciniphila* strains from human stool

A total of 32 fecal samples were obtained from the human dock center of the Asan Medical Center. The samples were collected from fresh residual samples after fecal occult blood and parasitic examination on the same date. Fecal samples were suspended in PBS and then seeded onto brain heart infusion agar without dextrose (Kisan-Bio, Seoul, South Korea) supplemented

with 0.4% mucin (BHI-M). The fecal cultures were maintained at 37°C under anaerobic conditions generated using a GasPak 100 system (BD Bioscience). Approximately 50 colonies were selected from BHI-M plates and tested with PCR for species-specific sequences with the primer set, 5′-CAGCACGTGAAGGTGGGGAC-3′ and 5′-CCTTGCGGTTGGCTTCAGAT-3′. *A. muciniphila* was isolated from 11 samples. One strain was established per sample by sub-culturing for future experimentation.

Oral administration of *A. muciniphila*

A. muciniphila (ATCC BAA-835^T) and newly isolated AK32 (KCTC 14172BP) strains were cultured in brain heart infusion media (BD Bioscience) supplemented with 0.4% mucin (Sigma) and maintained in an anaerobic incubator using the GasPak 100 system (BD Bioscience) at 37°C. Cultures were centrifuged, the culture pellet was suspended in anaerobic PBS, and the culture pellet was orally administered to mice (8×10^8 CFU per dose) every day for 4 weeks by a Zonde needle. Heat-inactivated BAA-835 was prepared by pasteurization for 30 min at 70°C (Plovier et al., 2017) and administered to mice orally (8×10^8 CFU per dose).

Treatment with irradiation and methotrexate

Mice were injected intraperitoneally with methotrexate (MTX; 120 mg/kg, Sigma) followed by administration of 10 Gy of total body irradiation (cesium source irradiator; Precision X-Ray, North Branford, CT).

Cell isolation

Mouse SIs were opened longitudinally and washed with PBS. To dissociate the crypts, tissues were incubated at 4°C in 1 mM EDTA in PBS for 30 min, washed in PBS, and then transferred into 5 mM EDTA in PBS for an additional 1 h of incubation at 4°C. Samples were then suspended in PBS and filtered by a 70-μm cell strainer (BD Falcon). To purify ISCs and Paneth cells from Lgr5-GFP mice, crypt-cell suspensions were dissociated using TrypLE Express (Thermo Fisher Scientific) for 10 min at 37°C. The dissociated cells were stained with the Live/Dead Cell Stain kit (Thermo Fisher Scientific) and anti-CD24 monoclonal antibody (Thermo Fisher Scientific). Cell sorting was performed using a FACS AriaIII cell sorter. ISCs were sorted as Lgr5-GFP^{hi} and Paneth cells were sorted as Lgr5-GFP^{-}CD24^{hi}, respectively.

Organoid culture

For construction of organoids, 200–500 crypts per well were suspended in Matrigel (Corning) as described (Sato et al., 2009). Complete ENR medium (all components from Thermo Fisher Scientific unless noted) were comprised of advanced DMEM/F12 (Gibco), antibiotic-antimycotic (×100), 1 mM N-acetyl cysteine (Sigma-Aldrich), B27 supplement, N2 supplement, EGF, Noggin (R&D Systems), R-spondin-1-conditioned medium, and Y-27632 (Sigma). Y-27632 was added to the ENR medium for the first 48–72 h of culture only and then removed during the medium change. The ENR medium was replaced every 2 to 3 days. Colon organoids were cultured in the ENR medium supplemented with Wnt3 conditioned media (WENR). Human colon organoids were cultured in WENR medium supplemented with gastrin, nicotinamide, A83-01, and SB202190 (all from Sigma) as described (Sato et al., 2011a). Isolated ISCs and Paneth cells were co-cultured in ENR medium supplemented with Jagged-1 (1 μM; Anaspec). Wnt-C59 (50 μM; Abcam) was used as a porcupine (PORCN) inhibitor.

The surface areas of SI and colon organoids were measured microscopically by taking several random non-overlapping photos of organoids in a well using an inverted microscope (Carl Zeiss). Each photo was analyzed using ImageJ software (NIH) and the Zen image program (Carl Zeiss). Organoid perimeters for area measurements were defined manually using automated ImageJ software.

Histology

Ileum tissues were removed, opened longitudinally, and formed into Swiss rolls. The tissue was then fixed in 4% paraformaldehyde (PFA) and embedded in paraffin. Tissue sections were stained with hematoxylin-eosin (H&E) or periodic acid-Schiff (PAS). Quantification of the crypt height and goblet cell number was carried out by blinded operators. Pathology scoring was conducted in a blinded fashion using a scoring system. In brief, two parameters were measured: extent of injury (0, none; 1, basal one-third damaged; 2, basal two-thirds damaged; 3, only surface epithelium intact; 4, entire crypt and epithelium lost) and crypt damage (0, none; 1, basal one-third damaged; 2, basal two-thirds damaged; 3, only surface epithelium intact; 4, entire crypt and epithelium lost). The sum of the two parameter values was multiplied by a factor that reflected the percentage of tissue involvement (1, 0 %~25 %; 2, 26 %~50 %; 3, 51 %~75 %; 4, 76 %~100 %).

Immunofluorescence staining

Ileum tissues were fixed with 4% PFA and dehydrated with 15%, and then 30% sucrose in PBS. Dehydrated tissues were formed into a Swiss roll, frozen, and sliced. For staining, collected organoids were permeabilized in PBS containing 0.1% Tween 20 and blocked with

0.5% BSA in PBS for 1 h. For Muc2 staining, ileum tissues containing feces were fixed in Carnoy's solution and embedded in paraffin. The primary antibodies used were rabbit anti-Muc2 (Abcam), rat anti-Ki67 (Biolegend), rabbit anti-lysozyme (Abcam), goat anti-Wnt3 (Abcam), mouse anti-β-catenin (BD Bioscience), and mouse anti-phospho-ERK1/2 (Thermo Fisher Scientific). Secondary antibodies were Alexa Fluor goat 594 anti-rat IgG (Biolegend), Alexa Fluor 488 goat anti-mouse IgG (Abcam), Alexa Fluor 546 donkey anti-goat IgG (Thermo Fisher Scientific), and Alexa Fluor 488 goat anti-rabbit IgG (Thermo Fisher Scientific).

RNA *in situ* hybridization

Tissues fixed in 4% PFA were used for RNA in situ hybridization, which was performed using the RNAscope 2.5 HD Detection Kits (ACD Bio) according to the manufacturer's instructions. RNA probes were designed by ACD Bio. The probe signal was detected by DAB (3.3'-diaminobenzidine).

Organoid treatment with cecal contents and bacterial culture supernatants

Cecal contents (100 mg) were diluted in 1 mL of serum-free DMEM/F12 (Gibco) medium and vortexed for 1 h. The contents were centrifuged at 4,000 rpm for 10 min and supernatants were passed through a 0.22-μm syringe filter (Pall Corp.) before cultivation. Bacterial culture supernatants were prepared by centrifuging at 12,000 rpm for 10 min and passing the supernatants through a 0.22-μm syringe filter (Pall Corp.). To address the effectiveness of cecal contents or bacteria culture supernatants in promoting organogenesis, I used ENR or WENR media supplemented with cecal content supernatant (0.01%) or bacterial culture

supernatant (4%) diluted in advanced DMEM/F12. For inhibition of Gpr41/43, I used Gpr43 antagonist (GLPG0974; 0.1 μM, Tocris) and Gpr41 antagonist (β-hydroxybutyrate, 3 mM; Sigma).

Microbiome data analysis pipeline

Total DNA was extracted from feces and SI contents using QIAamp DNA stool mini kits (Qiagen) in accordance with the manufacturer's instructions. For bacterial PCR amplification, primers targeting 341F and 805R were used. The amplified product was purified and sequenced by Chunlab (Seoul, South Korea) with an Illumina Miseq Sequencing system (Illumina). The processing of raw reads started with a quality check and filtering of low-quality (<Q25) reads by Trimmomatic software (ver. 032). After a quality control pass, paired-end sequence data were merged together using VSEARCH version 2.13.4 with default parameters. Non-specific amplicons that did not encode 16S rRNA were detected by nhmmer in the HMMER software package, version 3.2.1. I used the EzBioCloud 16S rRNA database for taxonomic assignment by precise pairwise alignment (Yoon et al., 2017). After chimeric filtering, reads that were not identified to the species level (with <97% similarity) in the EzBioCloud database were compiled. Operational taxonomic units with single reads (singletons) were omitted from further analysis. The alpha diversity (Shannon index) and beta diversity for the sample difference were estimated. A taxonomic cladogram was generated using LEfSe with a threshold of 2 on the logarithmic LDA score (Segata et al., 2011). A relationship based on a Pearson correlation between gut microbiota and SCFAs was visualized using Calypso software (Zakrzewski et al., 2017).

Whole-genome sequencing

The integrity of gDNA was tested by running an agarose gel electrophoresis. gDNA was quantified using the Quant-IT PicoGreen protocol (Invitrogen). The sequencing libraries were then prepared according to the manufacturer's instructions (20 kb template preparation and the BluePippinTM Size-Selection System) using the PacBio DNA template Prep Kit 1.0. The libraries were quantified using Quant-IT PicoGreen and qualified using a high-sensitivity DNA chip (Agilent Technologies). Subsequently, the libraries were sequenced using PacBio P6C4 chemistry in 8-well-SMART Cell v3 in PacBio RSII. The genome of the AK32 strain was constructed de novo using PacBio sequencing data. Sequencing analysis was performed by Chunlab. PacBio sequencing data were assembled with PacBio SMRT analysis 2.3.0 using the HGAP2 protocol (Pacific Biosciences). Resulting contigs from the PacBio sequencing data were circularized using Circlator 1.4.0 (Sanger Institute). The gene-finding and functional annotation pipeline of the whole-genome assembly was used from the EzbioCloud genome database. Protein-coding sequences were predicted by Prodigal 2.6.2 (Hyatt et al., 2010). Genes coding for tRNA were searched using tRNAscan-SE 1.3.1 (Schattner et al., 2005). I searched the rRNA and other non-coding RNAs in the Rfam 12.0 database (Nawrocki and Eddy, 2013). Comparative whole-genome analysis was studied by average nucleotide identity base BLAST (ANIb). The ANIb value was calculated by ANI calculator from the Kostas lab (http://enve-omics.ce.gatech.edu/ani).

Identification of *A. muciniphila* by carbohydrate fermentation pattern, enzymatic activity, and protein

I determined the carbohydrate fermentation pattern and enzymatic activity, respectively, of API 20A and API ZYM (BioMérieux, France) per the manufacturer's instructions. MALDI-TOF MS analysis using the Microflex LT/SH (Bruker, France) was used for protein-based identification. Bacteria were prepared for MALDI-TOF MS analysis by using ethanol/formic acid extraction methods according to the manufacturer's manual. Mass spectra were analyzed by MALDI Biotyper software package. Identification log scores were interpreted as recommended by the manufacturer. Log scoring was as follows: ≥2 and <3, high-confidence identification; ≥1.70 and <2, low-confidence identification; and ≥0 and <1.70, no organism identification possible.

Real-time PCR

Total RNA from the SI, LI, and SI-derived organoids was extracted using the RNeasy mini kit (Qiagen) and cDNA was synthesized using Superscript II reverse transcriptase and oligo dT primer (Thermo Fisher Scientific). Total RNA of *A. muciniphila* was extracted using Trizol (Thermo Fisher Scientific). The ReverTra Ace qPCR RT master mix with gDNA remover (Toyobo) was used to synthesize cDNA from bacterial RNA. cDNA was used as the template for real-time PCR performed using SYBR green chemistry (Thermo Fisher Scientific) on a Real-time PCR system (Applied Biosystems). The real-time PCR primers used in this study were as follows: *Muc2*, 5′-CCTTAGCCAAGGGCTCGGAA-3′ and 5′-GGCCCGAGAGTAGACCTTGG-3′; *Lyz1*, 5′-ATGGCGAACACAATGTCAAA-3′ and 5′-GCCCTGTTTCTGCTGAAGTC-3′; *Dll1*, 5′-CAGGACCTTCTTTCGCGTAT-3′ and 5′-AAGGGGAATCGGATGGGGTT-3′; *Math1*, 5′-GCCTTGCCGGACTCGCTTCTC-3′ and 5′-

TCTGTGCCATCATCGCTGTTAGGG-3′; *Spdef1*, 5′-CCGGTTGCCTGCTACTGTTC-3′ and 5′-GCCCATTGCTCCTGATGCT-3′; *Wnt3*, 5′-CTTCTAATGGAGCCCCACCT-3′ and 5′-GAGGCCAGAGATGTGTACTGC-3′; *Axin2*, 5′-AACCTATGCCCGTTTCCTCT-3′ and 5′-GAGTGTAAAGACTTGGTCCA-3′; *Ctnnb1*, 5′-ATGGAGCCGGACAGAAAAGC-3′ and 5′-TGGGAGGTGTCAACATCTTCTT-3′; *Lgr5*, 5′-CCTGTCCAGGCTTTCAGAAG-3′ and 5′-CTGTGGAGTCCATCAAAGCA-3′; *Notch1*, 5′-GCTGCCTCTTTGATGGCTTCGA-3′and 5′-CACATTCGGCACTGTTACAGCC-3′; *Hes1*, 5′-CCAGCCAGTGTCAACACGA-3′ and 5′-AATGCCGGGAGCTACTTTCT-3′; *β-actin*, 5′-TGGAATCCTGTGGCATCCATGAAAC-3′ and 5′-TAAAACGCAGCTCAGTAACAGTCCG-3′; *pdh*, 5′-AACCGATTATTGAAGCGGCA-3′and 5′-ATATTGGCGGCTTCGTGAAA-3′; *mmd*, 5′-GACCAAGAAGGAACGCCTCA-3′ and 5′-GTTCCGTCACCTTGCATTCG-3′; Universal 16S rDNA, 5′-ACTCCTACGGGAGGCAGCAG-3′ and 5′-ATTACCGCGGCTGCTGG-3′; and *A. muciniphila* 16S rDNA, 5′-CAGCACGTGAAGGTGGGGAC-3′ and 5′-CCTTGCGGTTGGCTTCAGAT-3′.

Quantitative measurement of SCFAs

All reagents and solvents for metabolite analysis were purchased from Sigma. Freeze-dried cecal contents (10 mg) were homogenized vigorously with 400 μL of internal standard solution [1 mM propionic acid (C3)-d6 and 100 μM butyric acid (C4)-d7] in water. For analysis of bacterial culture supernatant, I mixed 100 μL of culture supernatant with 200 μL of internal standard solution. After centrifuging, the supernatant was filtered out. AABD-SH (20 μL of 20 mM), TPP (20 μL of 20 mM), and DPDS (20 μL) in dichloromethane were added to the filtrate. The solution was incubated for 10 min at RT with vortexing and dried under vacuum. The sample was reconstituted with 80 μL of methanol prior to LC-MS/MS analysis. The LC-

MS/MS system was equipped with a 1290 HPLC (Agilent Technologies, Denmark), Qtrap 5500 (ABSciex), and a reverse-phase column (Pursuit 5 C18 150 × 2.0 mm; Agilent Technologies). The extracted ion chromatogram (EIC) corresponding to a specific transition for each metabolite was used for quantitation. The area under the curve of each EIC was normalized to the EIC of the internal standard. The peak area ratio of each metabolite was normalized to the internal standard using serum volume or tissue weight in a sample, and then used for relative comparison.

Statistical analysis

Statistical analyses were performed by using Prism software (GraphPad, La Jolla) with a two-tailed t-test and one-way analysis of variance (ANOVA) followed by Tukey's post hoc test. Data are presented as mean ± SEM. The values $p < 0.05$, $p < 0.01$, and $p < 0.001$ were considered statistically significant.

Result

Oral administration of *A. muciniphila* BAA-835 promotes epithelial differentiation in the SI.

To address whether mucin-degrading bacteria regulate IEC differentiation, BAA-835 was given orally to mice for 4 weeks. I first assessed the relative abundance of *A. muciniphila* in the SI contents of naïve B6 mice (Figure 6a). The relative abundance of *A. muciniphila* was about 0.037. Colonization of BAA-835 in the SI ileum was further confirmed by *in situ* hybridization (ISH) (Figure 6b). Mice treated with BAA-835 showed increased crypt height and higher numbers of mucin-producing goblet cells in the SI and colon than seen in mice treated with PBS (Figure 7a and 7b). Owing to the increased presence of goblet cells in response to BAA-835 treatment, protein and mRNA expression of mucin2 (Muc2) were examined in the SI. Muc2 is one of the glycosylated proteins mainly produced by goblet cell in the SI. Muc2 expression, along with mucus thickness, were significantly higher in the SI of BAA-835-treated mice than in PBS-treated control mice (Figure 8a and 8b). Additionally, administration of BAA-835 resulted in increased numbers of lysozyme-positive (Lyz^+) Paneth cells and mRNA expression of *Lyz1* in the crypt of the SI (Figure 9a and 9b). Paneth cells produce Lyz as antimicrobial peptide. Previous other study revealed that $Lgr5^+Ki67^-$ cells at crypt positions +4/+5 in the SI were found to differentiate into secretory lineage cells (Basak et al., 2014). As expected, BAA-835-treated mice had more $Lgr5^+Ki67^-$ cells at the +4/+5 crypt positions than PBS-treated mice (Figure 10a and 10b). Furthermore, I observed an increase in the expression of the transcription factors, *Dll1*, *Math1*, and *Spdef1*, that regulate differentiation of secretory lineage cells (Gregorieff et al., 2009; Van Es et al., 2012; Yang et al., 2001), in BAA-835-treated mice compared with controls (Figure 10c). These results suggest that *A. muciniphila* may promote differentiation of secretory lineage cells in the SI.

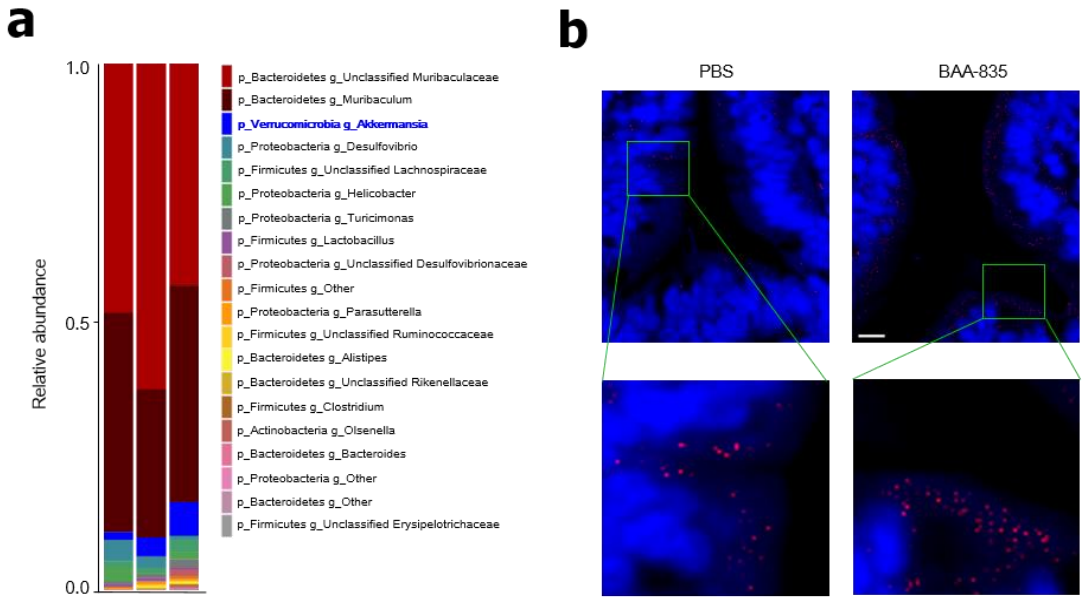

Figure 6. Bacteria colonization in SI after administration of *A. muciniphila* BAA-835.

(**a**) Microbiota composition of SI contents from naïve B6 mice at the genus level. (**b**) Fluorescence *in situ* hybridization of *A. muciniphila* in SI. Ileum tissues of mice were fixed in Carnoy's solution (methanol : chloroform : acetic acid = 6 : 3 : 1) and embedded in paraffin. Tissue sections were hybridized with the Cy-3-labeled fluorescence probe specific for *A. muciniphila* 16S rDNA (5′-CCTTGCGGTTGGCTTCAGAT-3′) in hybridization solution (20 mM Tris, pH 7.4, 0.9 M NaCl, 0.1% sodium dodecyl sulfate). Scale bars: 10 μm. n=3.

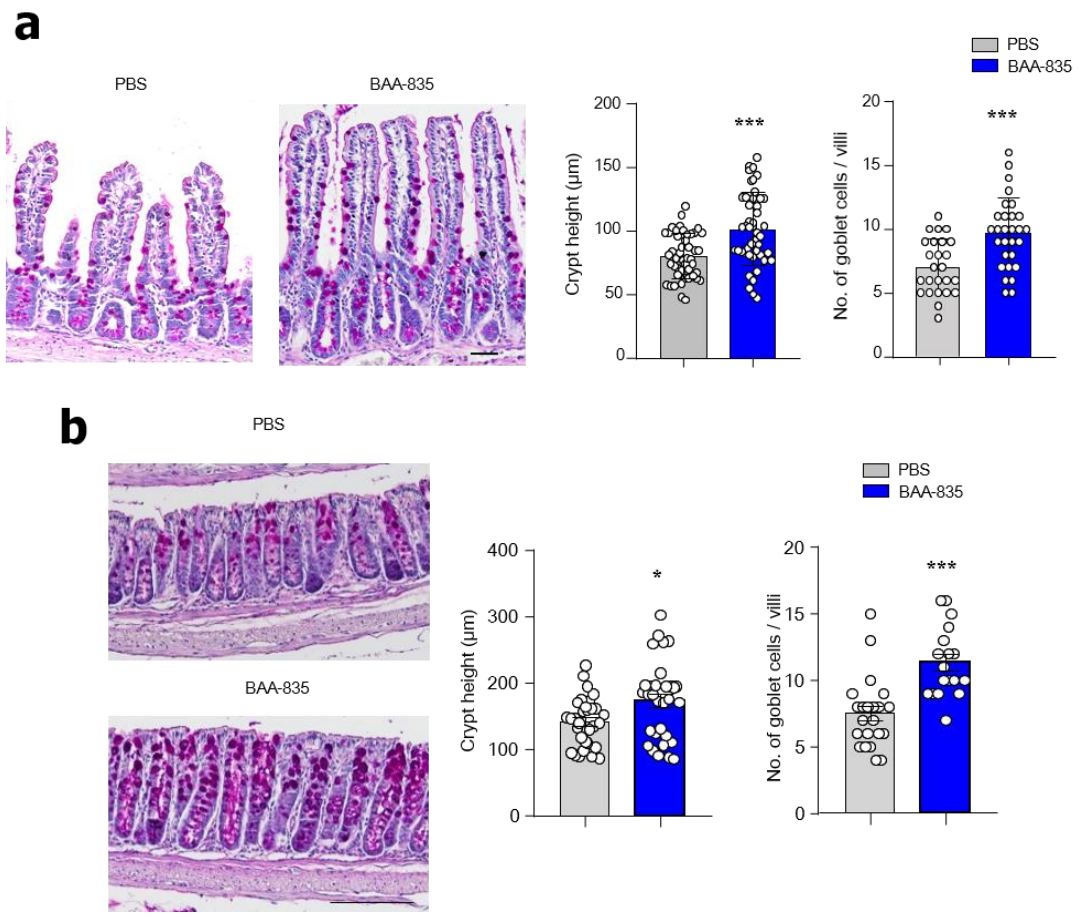

Figure 7. Oral administration with *A. muciniphila* BAA-835 enhanced epithelial development in the SI. (**a**) PAS staining of the SI and quantification of crypt heights and goblet cell numbers. (**b**) PAS staining of the colon and quantification of crypt heights and goblet cell numbers. Scale bars: 100 μm (a); 200 μm (b). Statistical analyses were done by two-tailed paired t-test. n=3-5. $^{*}p < 0.05$, $^{***}p < 0.001$. Data were combined from ≥3 independent experiments.

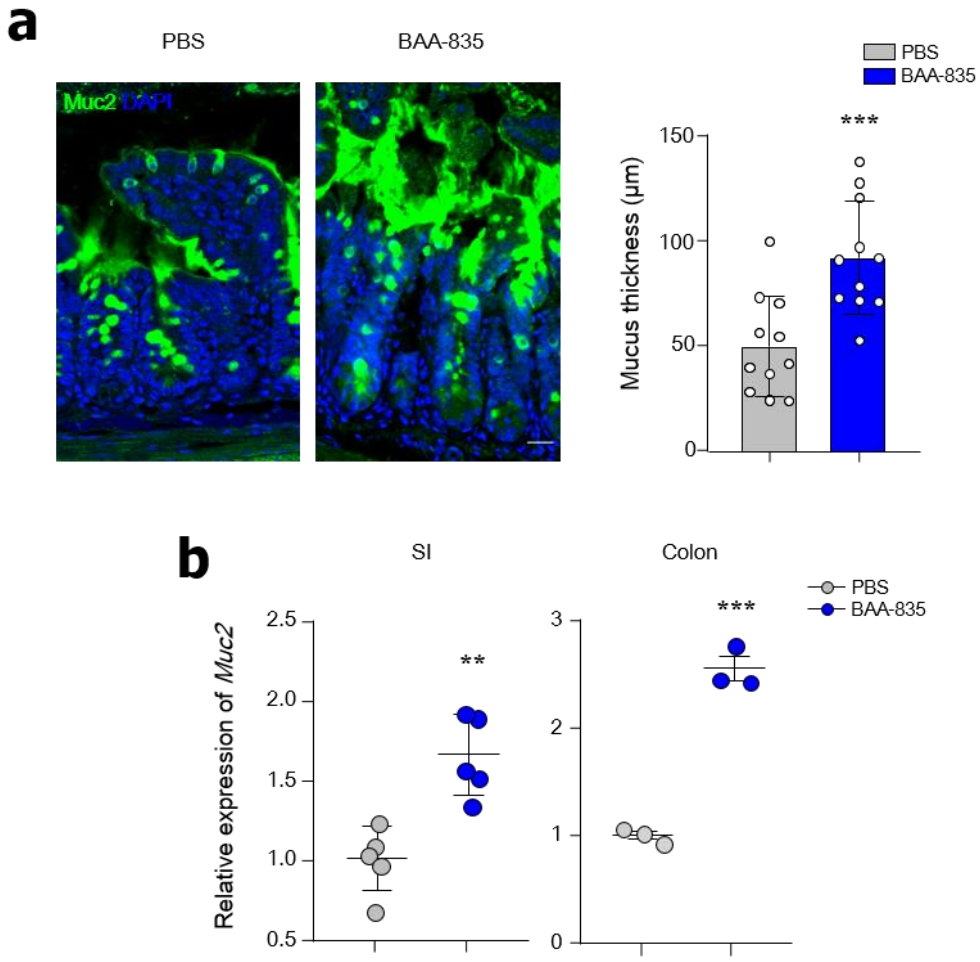

Figure 8. Oral administration with *A. muciniphila* BAA-835 accelerated a thicker layer of mucus in SI. (**a**) The SIs of mice treated with BAA-835 were fixed by water-free methanol Carnoy's fixative and stained with anti-Muc2 antibody to determine mucus thickness. (**b**) mRNA levels of *Muc2* in SI and colon. Scale bars: 20 μm (a). Statistical analyses were done by two-tailed paired t-test. n=3-5. $^{**}p < 0.01$, $^{***}p < 0.001$. Data were combined from ≥3 independent experiments.

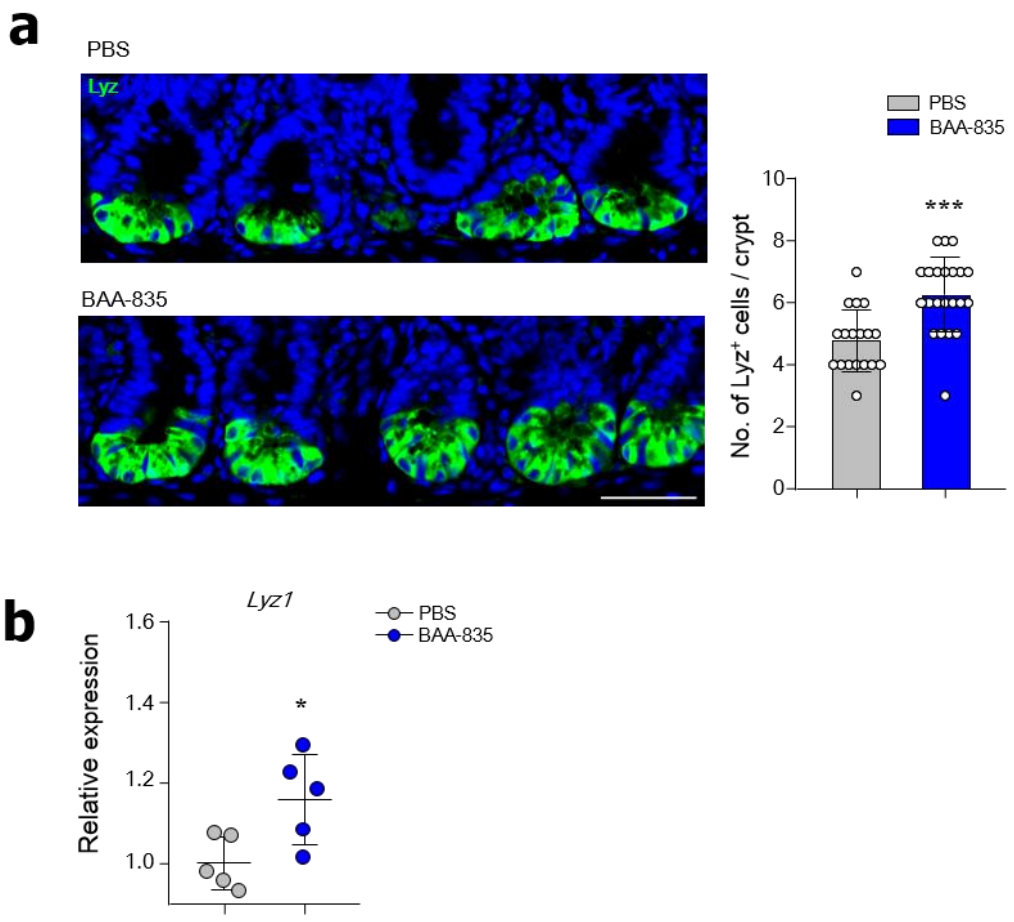

Figure 9. Oral administration with *A. muciniphila* BAA-835 increased Lysozyme expression. (**a**) Confocal image of Lysozyme^{+} Paneth cells and quantification. (**b**) mRNA levels of *Lyz1* in SI. Scale bars: 50 μm (a). Statistical analyses were done by two-tailed paired t-test. n=3-5. $^{*}p < 0.05$, $^{***}p < 0.001$. Data were combined from ≥3 independent experiments.

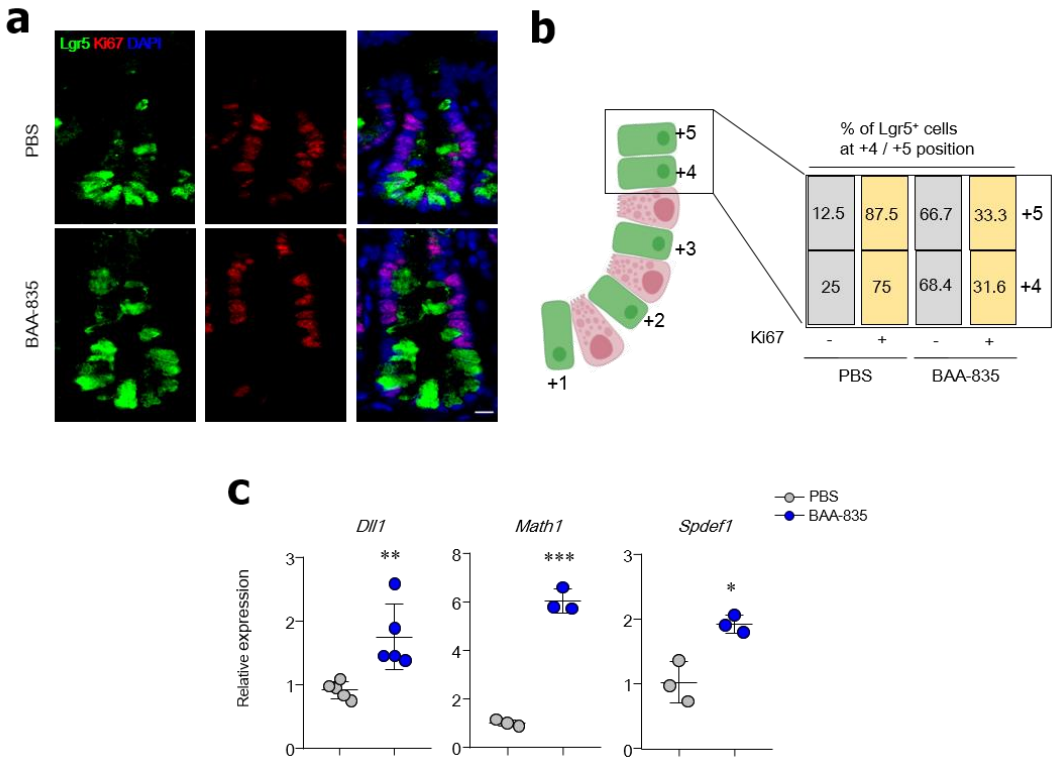

Figure 10. Oral administration with *A. muciniphila* BAA-835 promoted differentiation of secretory lineage cells in SI. (**a**) Confocal image of SI stained by anti-Ki67 antibody. (**b**) Percentages of Lgr5 GFP^{+} cells either expressing Ki67 or not in SI crypt. (**c**) mRNA levels of *Dll1*, *Math1*, and *Spdef1*. Scale bars: 5 μm (a). Statistical analyses were done by two-tailed paired t-test. n=3-5. $^{*}p < 0.05$, $^{**}p < 0.01$, $^{***}p < 0.001$. Data were combined from ≥3 independent experiments.

Oral administration of *A. muciniphila* BAA-835 accelerates ISC proliferation.

As secretory subtypes of IECs are derived from $Lgr5^+$ ISCs, I next investigated whether *A. muciniphila* modulates the proliferation of $Lgr5^+$ ISCs. Lgr5-GFP mice that were administered BAA-835 had more GFP-expressing $Lgr5^+$ ISCs in the SI and colon crypt than PBS-treated mice (Figure 11). Organoids derived from the SI and colon crypt of BAA-835-treated mice were larger than those of PBS-treated mice (Figure 12). Furthermore, Lgr5 expression was upregulated in the SI, SI organoids, and colon of BAA-835-treated mice compared with controls (Figure 13). RNA ISH analysis indicated increased numbers of $Olfm4^+$ cells, another marker of ISCs, in the SI crypt of BAA-835-treated mice (Figure 14). In addition, protein and mRNA levels of *Muc2* and *Lyz1* were upregulated in the SI organoids of BAA-835-treated mice compared with PBS-treated mice (Figure 15). These results imply that *A. muciniphila* may play a critical role in accelerating the proliferation of ISCs.

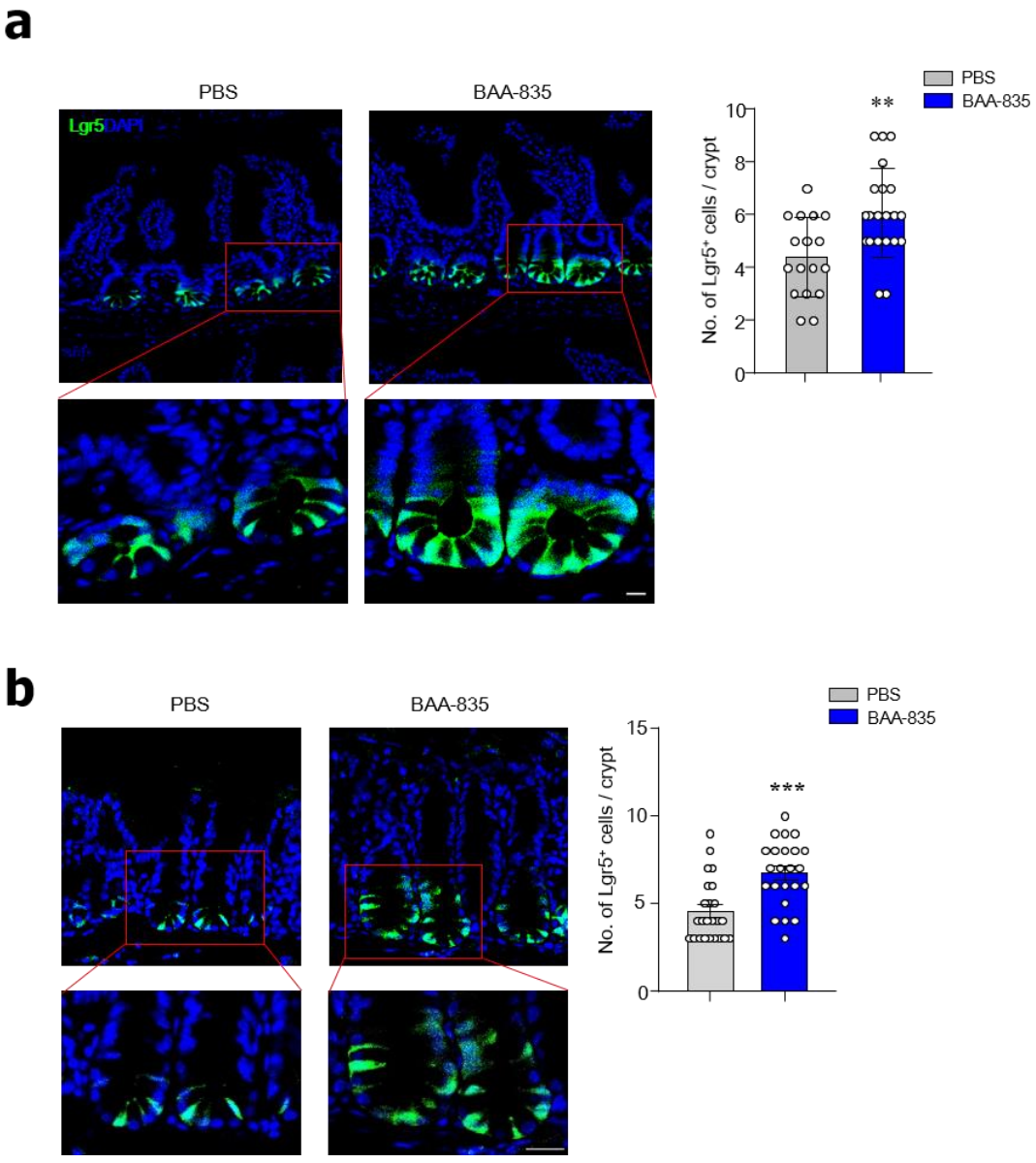

Figure 11. Oral administration with *A. muciniphila* BAA-835 showed enhanced Lgr5$^+$ stem cell populations in SI and colon. Confocal images of Lgr5 GFP cells and quantification of Lgr5 GFP cells in SI (**a**) and colon (**b**) crypts. Scale bars: 5 μm (a); 20 μm (b). Statistical analyses were done by two-tailed paired t-test. n=3-5. $^{**}p < 0.01$, $^{***}p < 0.001$. Data were combined from ≥2 independent experiments.

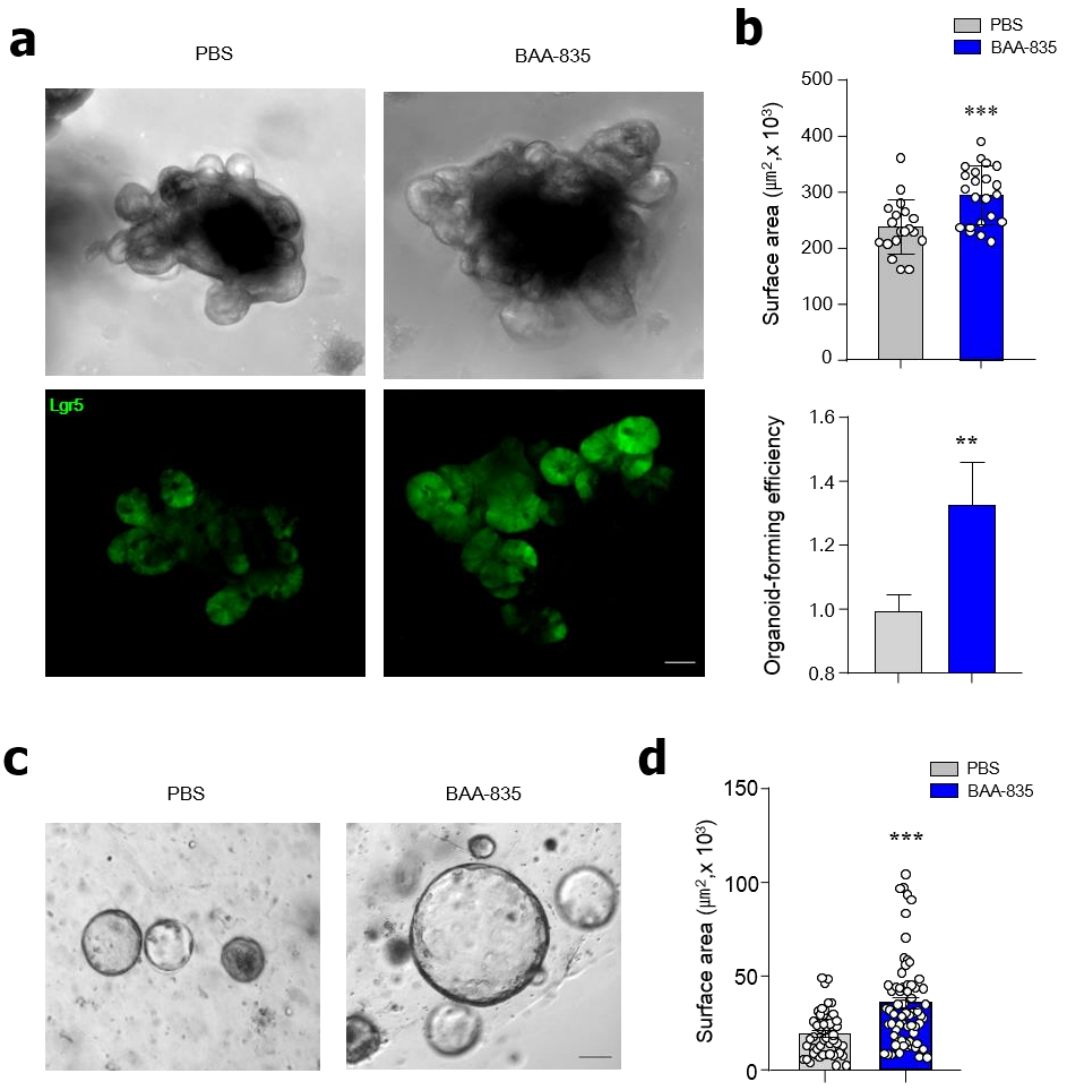

Figure 12. Oral administration with *A. muciniphila* BAA-835 enhanced organogenesis in SI and colon organoids. Lgr5 GFP expression (**a**) and surface areas for determining organoid-forming efficiency (**b**) of SI organoids. Representative bright-field image (**c**) and surface area (**d**) of colon-derived organoids. Scale bars: 5 μm (a); 20 μm (b). Statistical analyses were done by two-tailed paired t-test. n=3-5. $^{**}p < 0.01$, $^{***}p < 0.001$. Data were combined from ≥2 independent experiments.

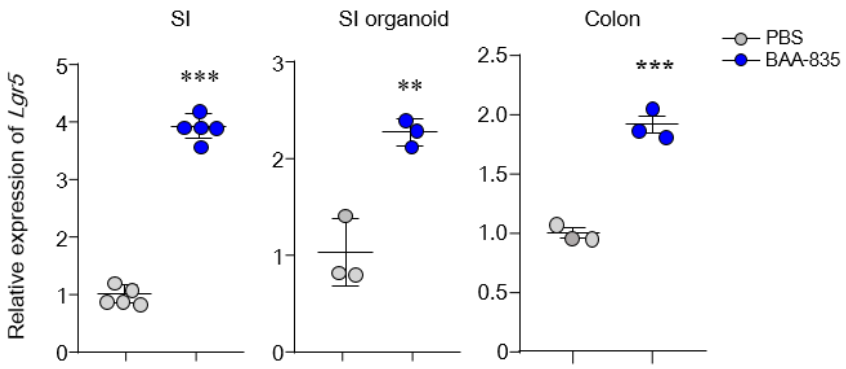

Figure 13. Oral administration with *A. muciniphila* BAA-835 accelerated expression of *Lgr5* in SI, SI organoid, and colon. mRNA levels of *Lgr5* in SI, SI organoid, and colon. Statistical analyses were done by two-tailed paired t-test. n=3-5. $^{**}p < 0.01$, $^{***}p < 0.001$. Data were combined from ≥2 independent experiments.

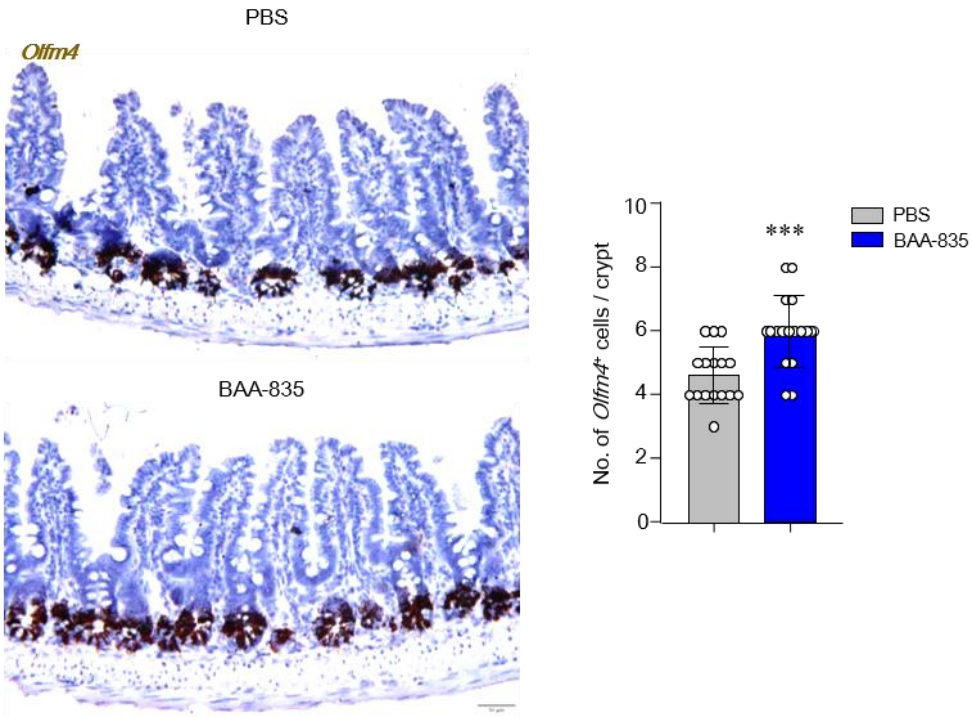

Figure 14. Oral administration with *A. muciniphila* BAA-835 increased numbers of *Olfm4*$^{+}$ cells in SI crypt. RNA *in situ* hybridization for *Olfm4* and quantification of *Olfm4*$^{+}$ cells in SI. Statistical analyses were done by two-tailed paired t-test. n=3-5. $^{***}p < 0.001$. Data were combined from ≥2 independent experiments.

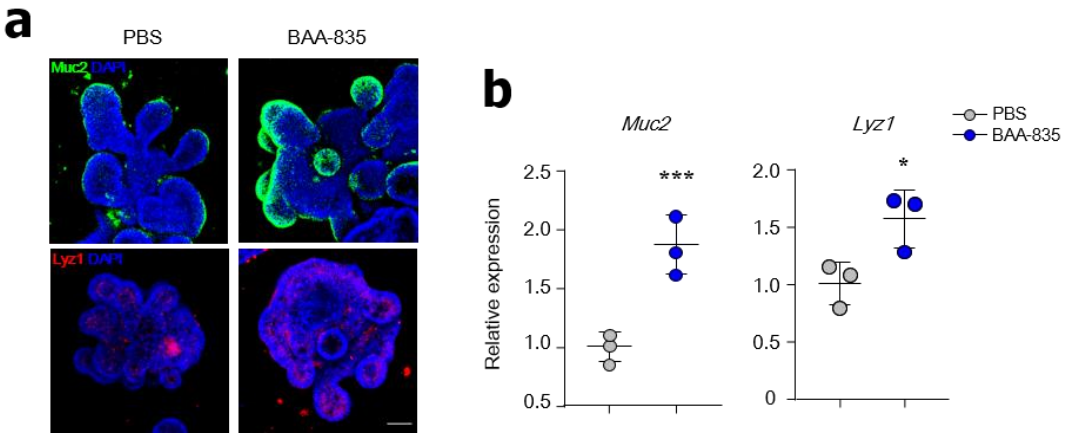

Figure 15. SI organoids of *A. muciniphila* BAA-835-treated mice showed upregulated protein and mRNA levels of *Muc2* and *Lyz1*. (**a**) Confocal image of SI organoid stained by anti-Muc2 and anti-Lyz antibodies. (**b**) mRNA levels of *Muc2* and *Lyz1* in SI organoids. Scale bars: 50 μm (Muc2); and 20 μm (Lyz1) (a). Statistical analyses were done by two-tailed paired t-test. n=3-5. $^{*}p < 0.05$, $^{***}p < 0.001$. Data were combined from ≥2 independent experiments.

Oral administration of *A. muciniphila* BAA-835 enhances ISC proliferation by Wnt signaling.

As Wnt and Notch signaling are involved in maintaining ISC stemness in the SI crypt, I next investigated whether *A. muciniphila* treatment regulates those pathways. Mice given BAA-835 orally had increased expression of *Wnt3*, *Axin2*, *Ctnnb1*, *Notch1*, and *Hes1* in their SI tissues (Figure 16a). Although both Wnt (*Wnt3*, *Axin2*, *Ctnnb1*) and Notch (*Notch1* and *Hes1*) signaling were activated by oral BAA-835, I focused on the Wnt-related signal because previous studies suggested the most important pathway for IEC development is Wnt signaling (Korinek et al., 1998; Van der Flier and Clevers, 2009). The upregulated expression of *Wnt3* and *Axin2* in the SI crypt of BAA-835-treated mice was further confirmed by RNA ISH (Figure 16b). In addition, Wnt3 protein levels were higher in the SI crypt and SI organoids of BAA-835-treated mice than in PBS-treated control mice (Figure 16c and 16d). Of note, β-catenin protein levels were upregulated in the nuclei of the SI crypt of BAA-835-treated mice compared with PBS-treated mice (Figure 17a), therefore indicating increased translocation from the cytoplasm. As the Wnt/β-catenin pathway activates RAS-ERK signaling that in turn promotes stemness (Wong et al., 2012), I next examined ERK phosphorylation (pERK) in the SI crypt. As expected, oral administration of BAA-835 increased pERK expression in the SI crypt compared with controls (Figure 17b). To address whether *A. muciniphila* activates Wnt3 signaling in the SI, Lgr5-GFP^{hi} ISCs isolated from naive mice were co-cultured with Paneth cells isolated from BAA-835-treated or PBS-treated mice. Interestingly, SI organoids grew significantly more in co-cultures isolated from BAA-835-treated mice than in PBS-treated mice (Figure 18). This effect was diminished when the porcupine inhibitor (Wnt-C59) was added to the co-cultures (Figure 18). Together, these findings demonstrate that *A. muciniphila* promotes the secretion of Wnt3 from Paneth cells that support ISC proliferation in the SI.

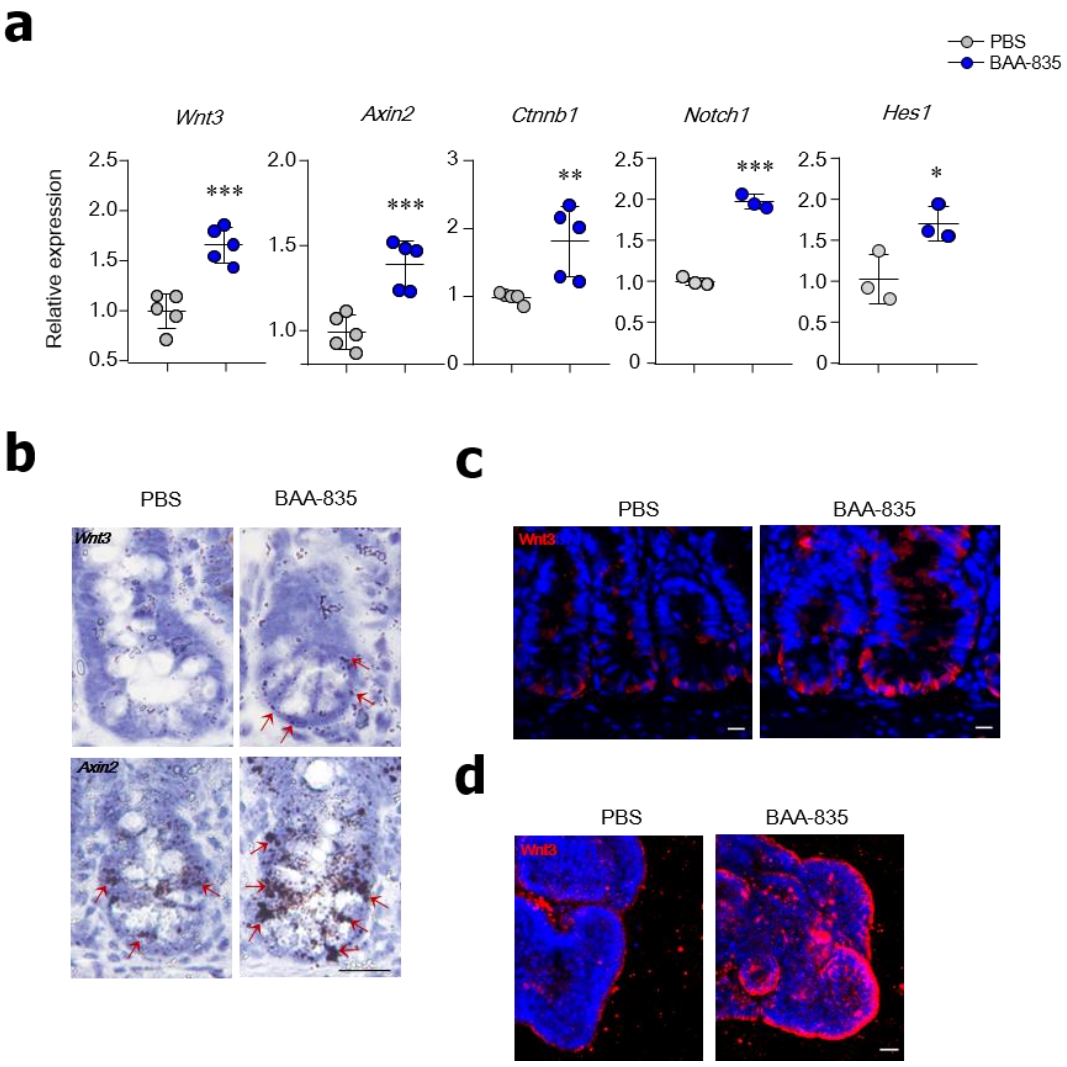

Figure 16. Oral administration with *A. muciniphila* BAA-835 activated Wnt and Notch signaling. (**a**) mRNA levels of *Wnt3*, *Axin2*, *Ctnnb1*, *Notch1*, and *Hes1* in SI tissues. (**b**) *In situ* hybridization for *Wnt3* and *Axin2* in SI crypts. (**c**) Representative confocal images of Wnt3 in SI. (**d**) Representative confocal image of SI-derived organoid stained by anti-Wnt3 antibody. Scale bars: 10 μm (b); 20 μm (c); 50 μm (d). Statistical analyses were done by two-tailed paired t-test. n=3-5. $^{*}p < 0.05$, $^{**}p < 0.01$, $^{***}p < 0.001$. Data were combined from ≥3 independent experiments.

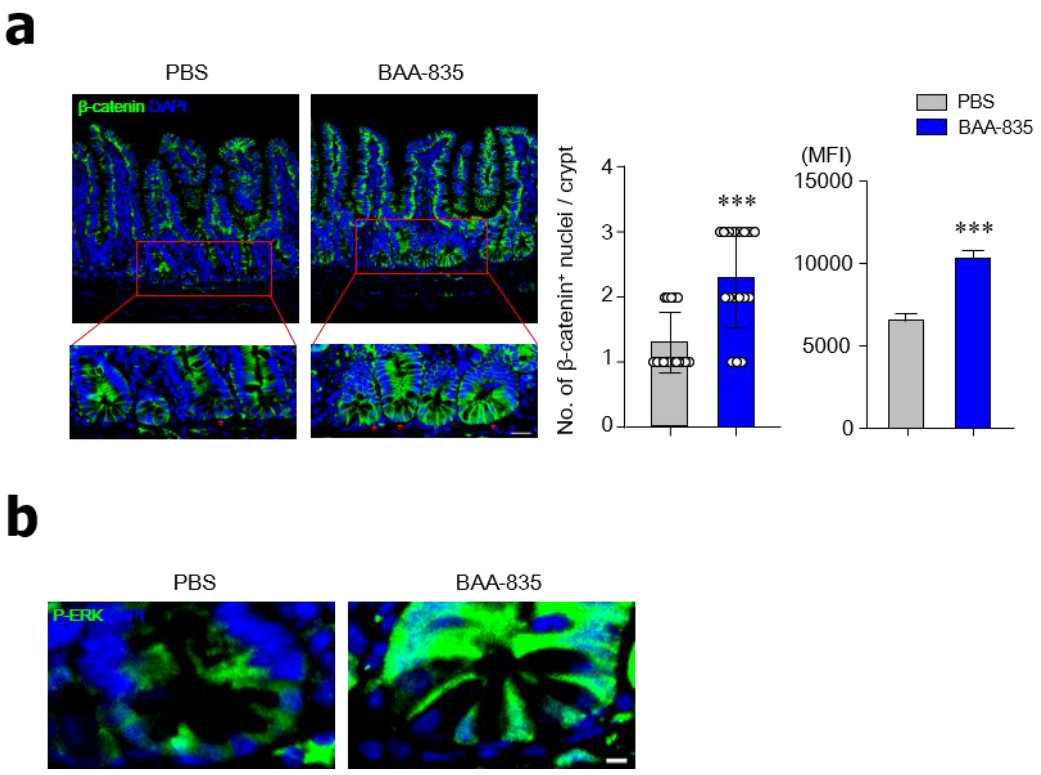

Figure 17. Oral administration with *A. muciniphila* BAA-835 activated Wnt/β-catenin pathway. (**a**) Representative confocal images of β-catenin in SI (left); numbers of nuclear translocation and mean fluorescence intensity (MFI) of β-catenin (right). (**b**) Representative confocal image of SI tissue stained by anti-P-ERK antibody. Scale bars: 20 μm (a); 20 μm (b). Statistical analyses were done by two-tailed paired t-test. n=3-5. $^{***}p < 0.001$. Data were combined from ≥3 independent experiments.

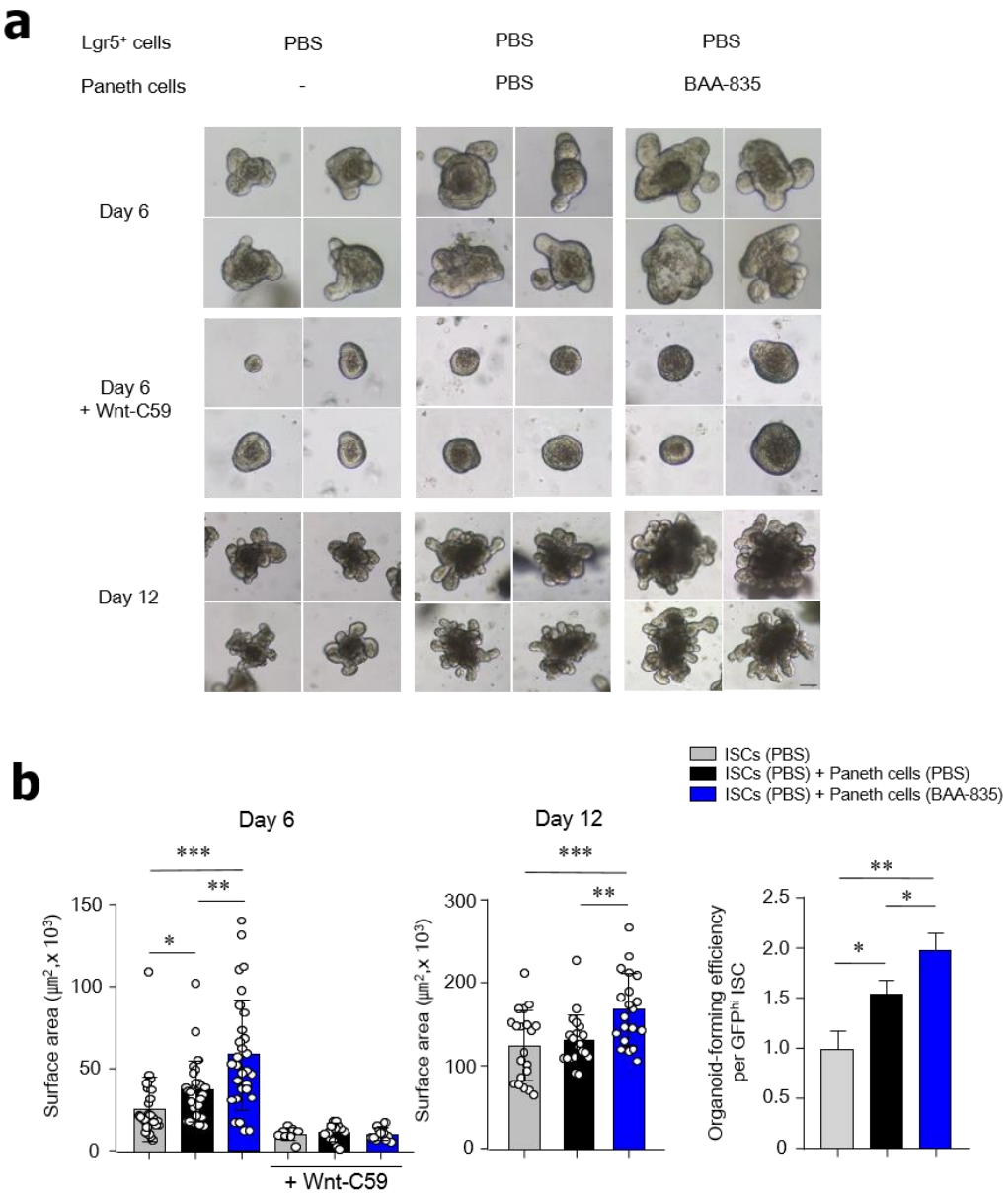

Figure 18. Oral administration with *A. muciniphila* promotes the secretion of Wnt3 from Paneth cells. (**a**) Co-culture with Lgr5 GFP ISCs and Paneth cells in the presence of Wnt-C59. (**b**) Surface area of the organoids was scored 6 and 12 days after plating for determining organoid-forming efficiency on Day 6. Scale bars: 20 μm on Day 6 and 50 μm on Day 12 (a). Statistical analyses were done by two-tailed paired t-test. n=3-5. $^{*}p < 0.05$, $^{**}p < 0.01$, $^{***}p < 0.001$. Data were combined from ≥3 independent experiments.

Oral administration of *A. muciniphila* BAA-835 promotes SCFA secretion and ISC-mediated epithelial development.

Based on the fact that microbiota-derived metabolites are a key factor in gut homeostasis, I next investigated whether metabolites produced from *A. muciniphila* treatment affected ISC-mediated epithelial development. To address this question, cecal contents from PBS- or BAA-835-treated mice were isolated and then applied to SI and colon organoids from naïve B6 mice and humans. Mouse SI and colon organoids, and human colon organoids treated with cecal contents from BAA-835-treated mice were significantly larger than those from PBS-treated one (Figure 19). Furthermore, mRNA levels of *Lgr5*, *Lyz1*, *Muc2*, and Wnt-related genes (i.e., *Wnt3*, *Axin2*, *Ctnnb1*) increased in presence of cecal contents obtained from BAA-835-treated mice compared with PBS-treated mice (Figure 20). To identify which metabolites are associated with *A. muciniphila*-mediated epithelial development, levels of SCFAs were examined in cecal contents. As expected, higher levels of SCFAs, including acetic, propionic, and butyric acids, were found in cecal contents of BAA-835-treated mice than in PBS-treated mice (Figure 21). Of these, acetic and propionic acids, but not butyric acid, were highly associated with increased SI organoid growth (Figure 22). Treatment with the Gpr41/43 antagonist that block effects of acetic and propionic acid on cells reduced SI organoid growth and forming efficiency (Figure 23), suggesting that BAA-835-derived SCFA metabolites play an important role in ISC-mediated epithelial development. In support of indispensable role of BAA-835-derived secretory components, I found that oral administration of heat-inactivated BAA-835 completely eliminated the ability to activate genes related to ISC-mediated epithelial development (Figure 24).

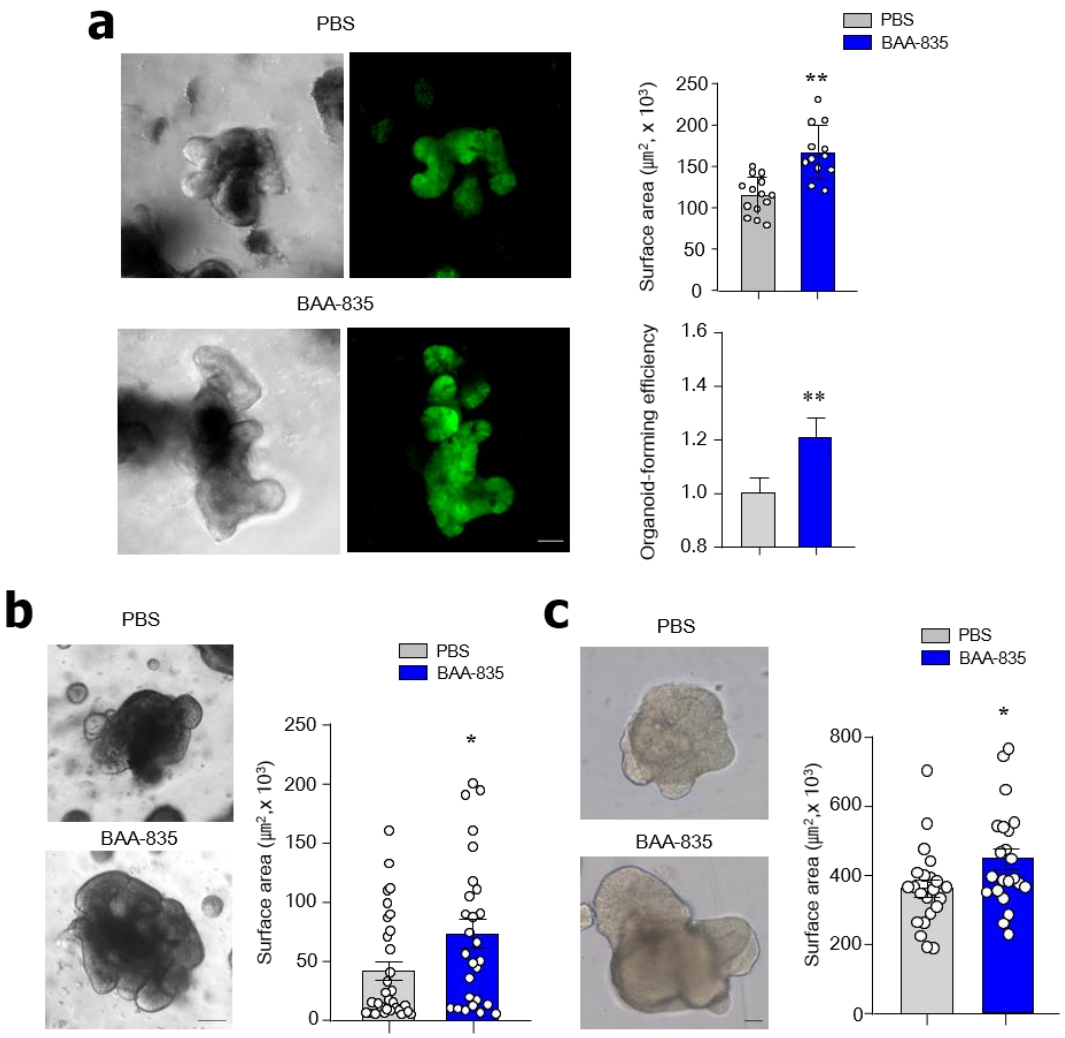

Figure 19. *A. muciniphila* BAA-835-derived metabolites promote organogenesis of SI and colon. (**a**) Lgr5 GFP expression and surface areas for determining organoid-forming efficiency of SI organoids in the presence of cecal contents. (**b**) Surface area of mouse colon organoid in the presence of cecal contents. (**c**) Surface area of human colon organoid in the presence of cecal contents. Scale bars: 50 μm (a); 100 μm (b); 100 μm (c). Statistical analyses were done by two-tailed paired t-test. n=3-5. $^{*}p < 0.05$, $^{**}p < 0.01$. Data were combined from ≥3 independent experiments.

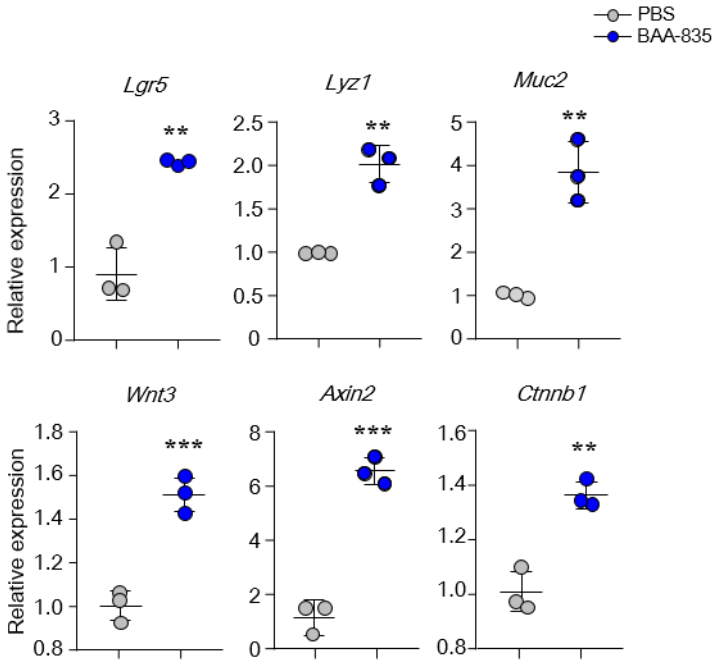

Figure 20. *A. muciniphila* BAA-835-derived metabolites increased organogenesis related gene expression. mRNA levels of *Lgr5*, *Lyz1*, *Muc2*, *Wnt3*, *Axin2*, and *Ctnnb1* in SI organoids treated with cecal contents. Statistical analyses were done by two-tailed paired t-test. n=3-5. $^{**}p < 0.01$, $^{***}p < 0.001$. Data were combined from ≥3 independent experiments.

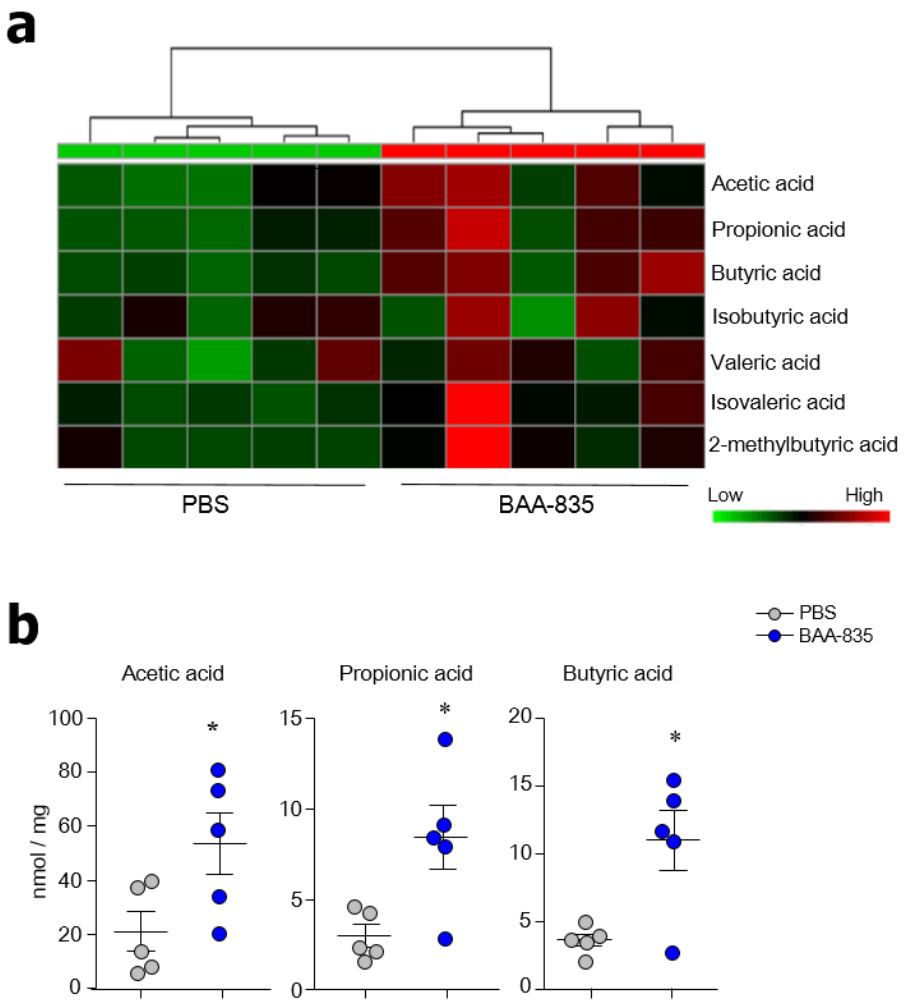

Figure 21. Higher levels of SCFAs were found in cecal contents of *A. muciniphila* BAA-835-treated mice. Heat map of SCFA (**a**) and quantification of acetic, propionic, and butyric acids (**b**) derived from cecal contents. Statistical analyses were done by two-tailed paired t-test. n=3-5. $^{*}p < 0.05$. Data were combined from ≥3 independent experiments.

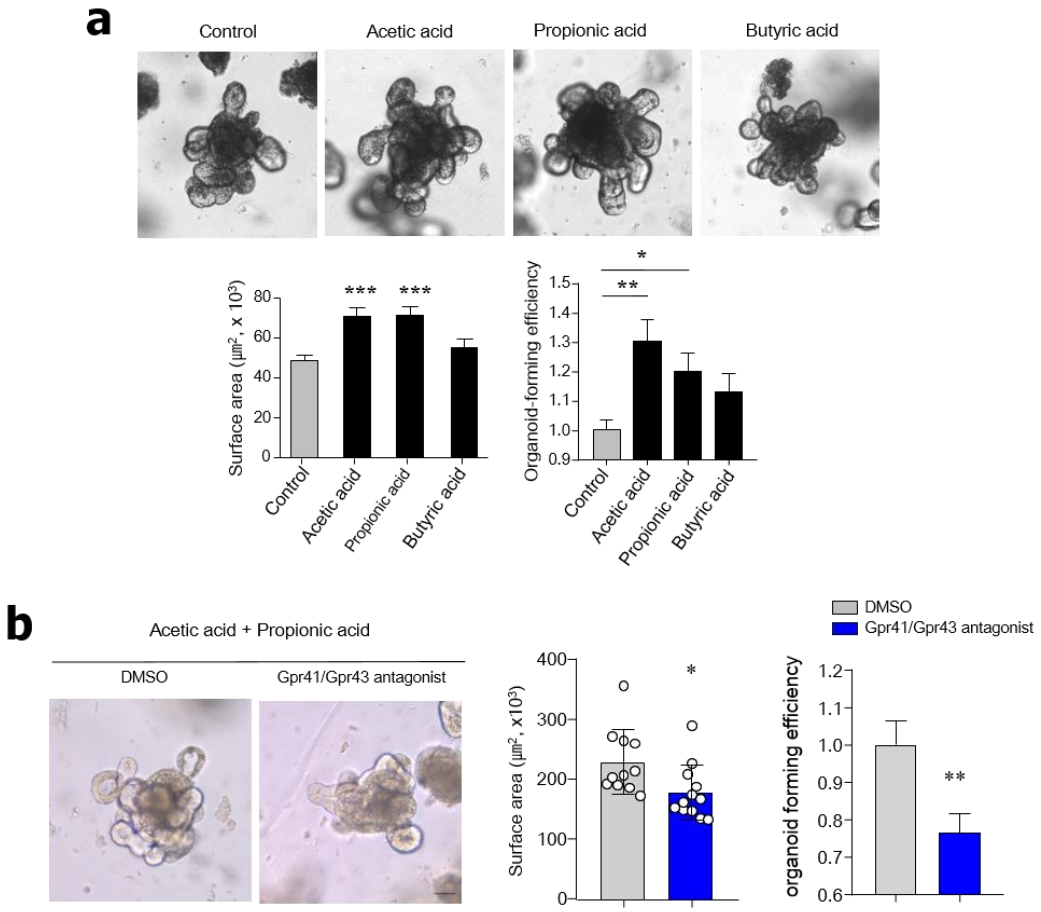

Figure 22. SI organoid growth measured after SCFA treatment. Representative bright-field image, surface area, and forming efficiency of SI-derived organoids. (**a**) Treatment with 0.5 mM acetic, propionic, or butyric acids. (**b**) Treatment with acetic and propionic acids in the absence or presence of Gpr41/43 antagonists. Scale bars: 50 µm (a); 100 µm (b). Statistical analyses were performed by one-way ANOVA with post hoc Tukey's test (a) and two-tailed paired t-test (b). n=3. $^{*}p < 0.05$, $^{**}p < 0.01$, $^{***}p < 0.001$.

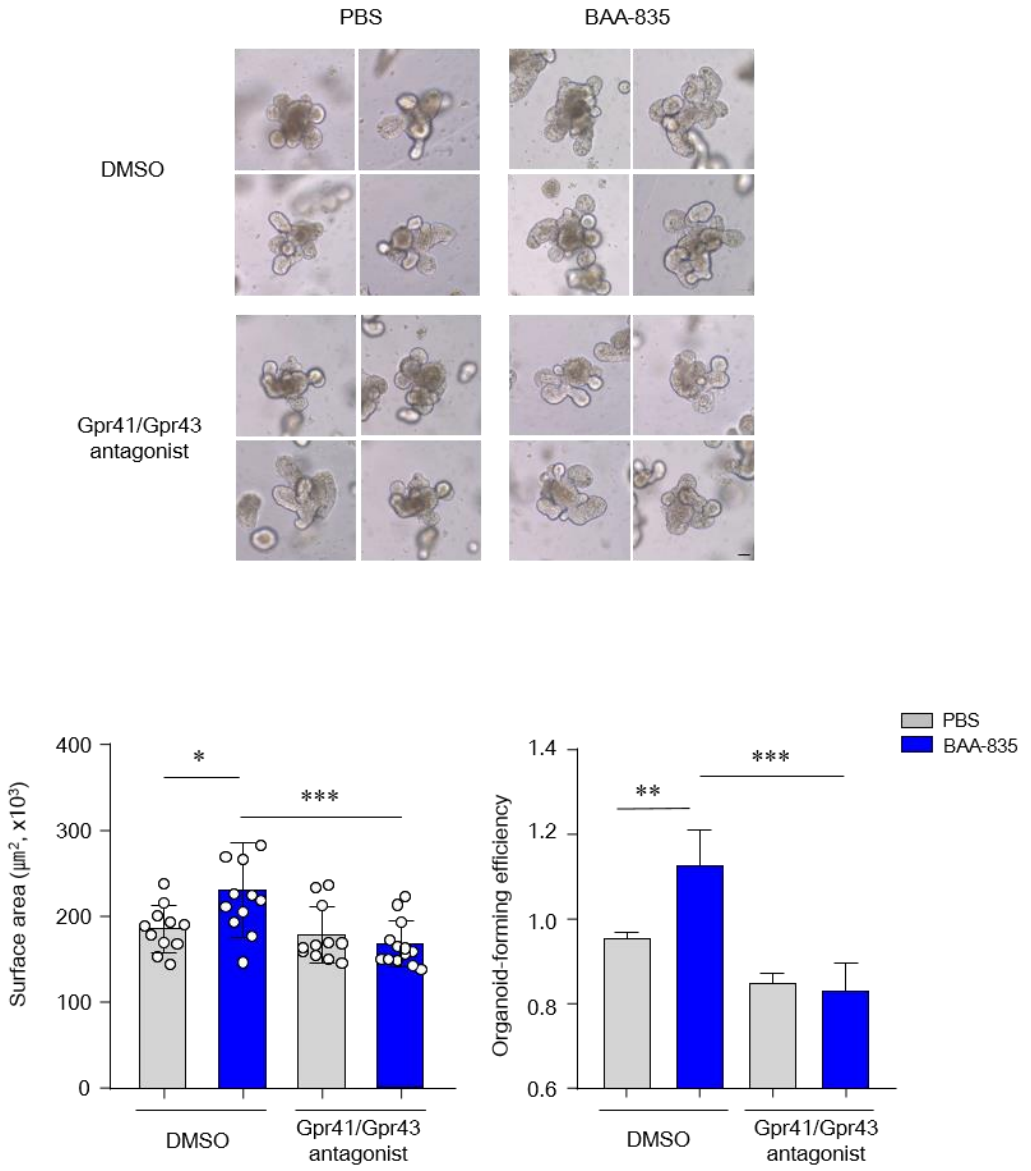

Figure 23. Treatment with Gpr41/43 antagonist reduced SI organogenesis. Representative bright-field image, surface area, and forming efficiency of SI-derived organoid treated with cecal contents in the absence or presence of Gpr41/43 antagonists. Statistical analyses were performed by one-way ANOVA with post hoc Tukey's test. n=3-5. $^{*}p < 0.05$, $^{**}p < 0.01$, $^{***}p < 0.001$. Data were combined from ≥3 independent experiments.

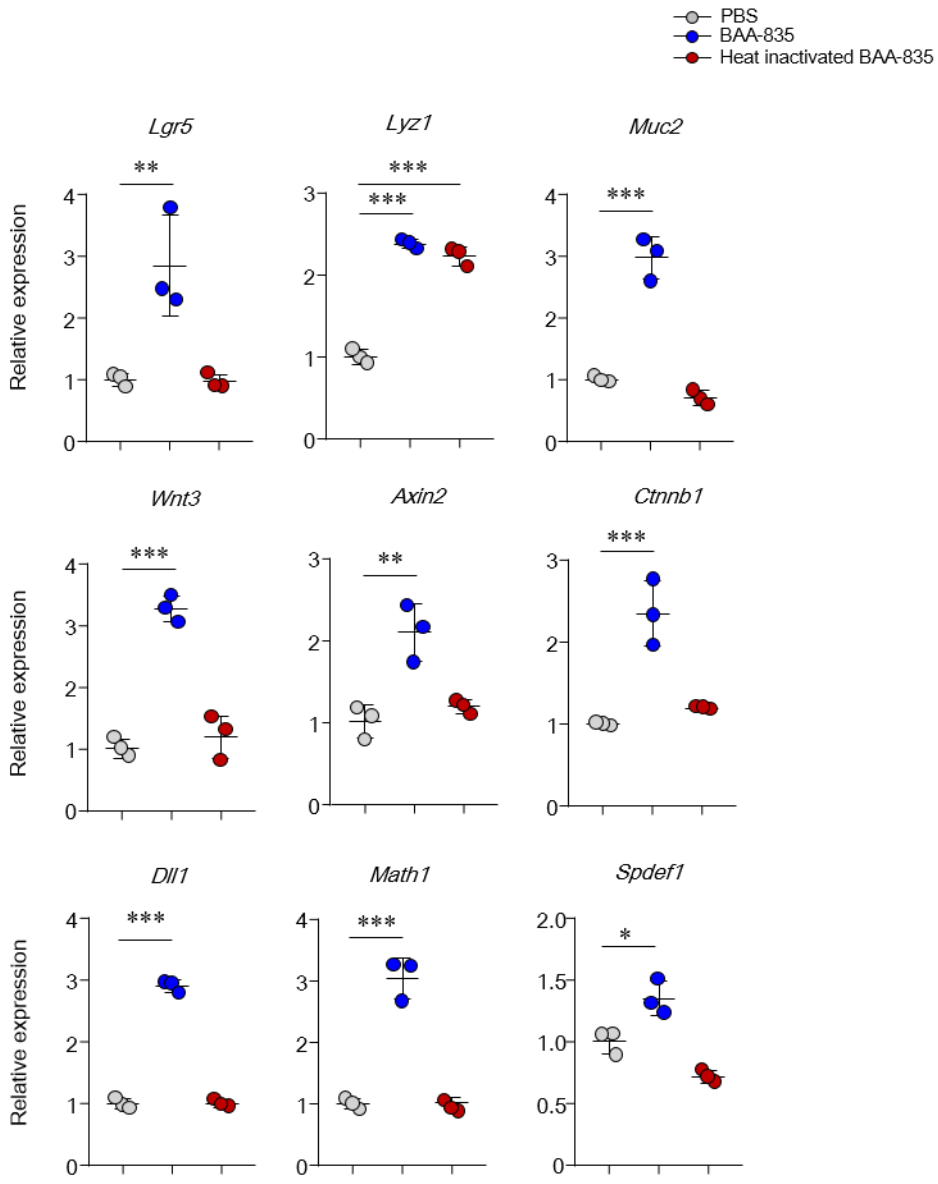

Figure 24. Effectiveness of pasteurized *A. muciniphila* BAA-835 on ISC-mediated epithelial development. Mice treated with heat-inactivated BAA-835 strain (8 x 10^8 CFU per dose) every day for four weeks. mRNA levels of *Lgr5, Lyz1, Muc2, Wnt3, Axin2, Ctnnb1, Dll1, Math1,* and *Spdef1* were addressed in SI tissues. Statistical analyses were carried out by one-way ANOVA with post hoc Tukey's test. n=3. $^{*}p < 0.05$, $^{**}p < 0.01$, $^{***}p < 0.001$.

Oral administration of *A. muciniphila* BAA-835 alters gut microbiota composition and SCFA production

I next addressed whether oral administration of *A. muciniphila* altered the composition of gut microbiota and found that it did (Figure 25a). At the phylum level, the gut microbiota from BAA-835-treated mice exhibited an increased proportion of the phyla Bacteroidetes and Proteobacteria and decreased numbers of the phyla Firmicutes compared with PBS-treated mice (Figure 25b). Further, linear discriminant analysis (LDA) with LEfSe confirmed that several bacterial genera were prominently changed after BAA-835 treatment (Figure 26a). The genera *Muribaculum*, *Alistipes*, *Akkermansia*, *Helicobacter*, and *Desulfovibrio* showed an upper 2 LDA score after BAA-835 treatment compared with control mice (Figure 26b). Furthermore, the Shannon index (α-diversity) that describe diversity within a particular group was significantly increased in BAA-835-treated mice compared with PBS-treated mice, indicating alteration of the bacterial community structure (Figure 27a). Unifrac-based PCoA analysis (β-diversity) that compares diversity between groups demonstrated that the two groups were clustered separately (Figure 27b). Interestingly, there was a positive correlation between the BAA-835-induced population and the presence of SCFA metabolites (i.e., acetic, propionic, and butyric acids) (Figure 27c). In summary, *A. muciniphila* treatment might promote ISC-mediated epithelial development by altering the gut microbiota composition, which in turn activates SCFA secretion.

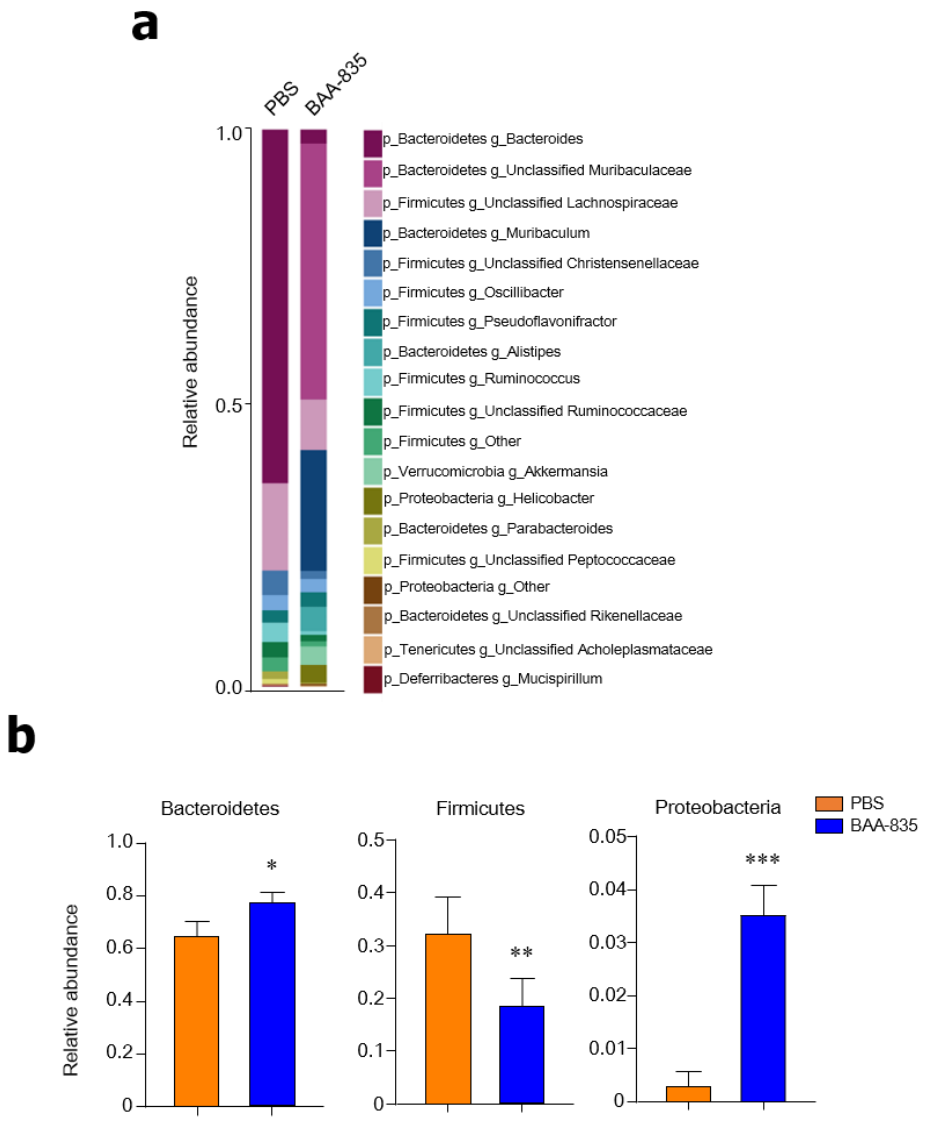

Figure 25. Microbiota composition in feces from *A. muciniphila* BAA-835-treated mice. (**a**) Fecal microbiota composition at the genus level. (**b**) Relative abundance of the phyla, Bacteroidetes, Firmicutes, and Proteobacteria. Statistical analyses were performed by two-tailed paired t-test. n=4. $^{*}p < 0.05$, $^{**}p < 0.01$, $^{***}p < 0.001$. Data were combined from ≥2 independent experiments.

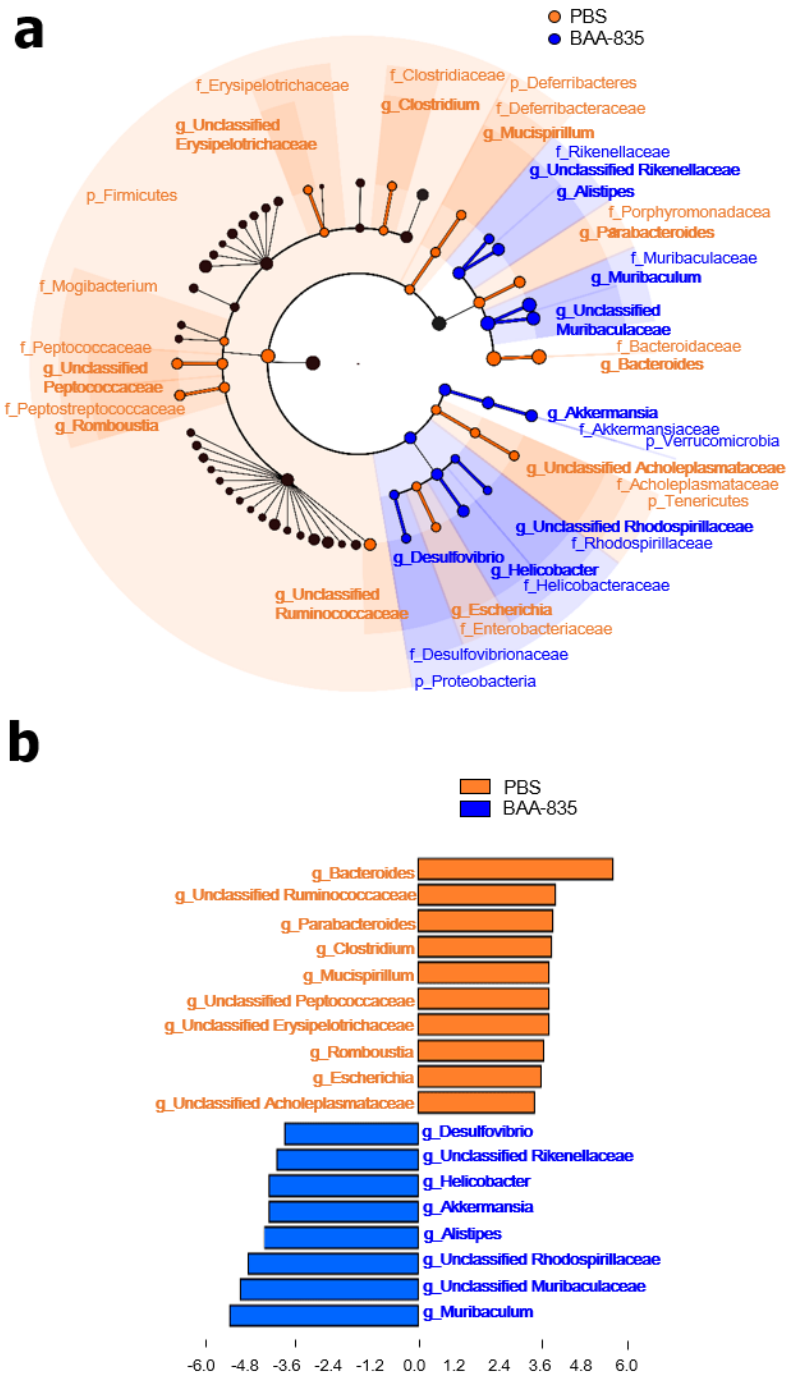

Figure 26. Oral administration of *A. muciniphila* BAA-835 results in change of gut microbiota composition. (**a**) Taxonomic cladogram from LEfSe. Dot size is proportional to taxon abundance. (**b**) LDA scores of differentially abundant taxa in fecal microbiome. LDA score > 2.

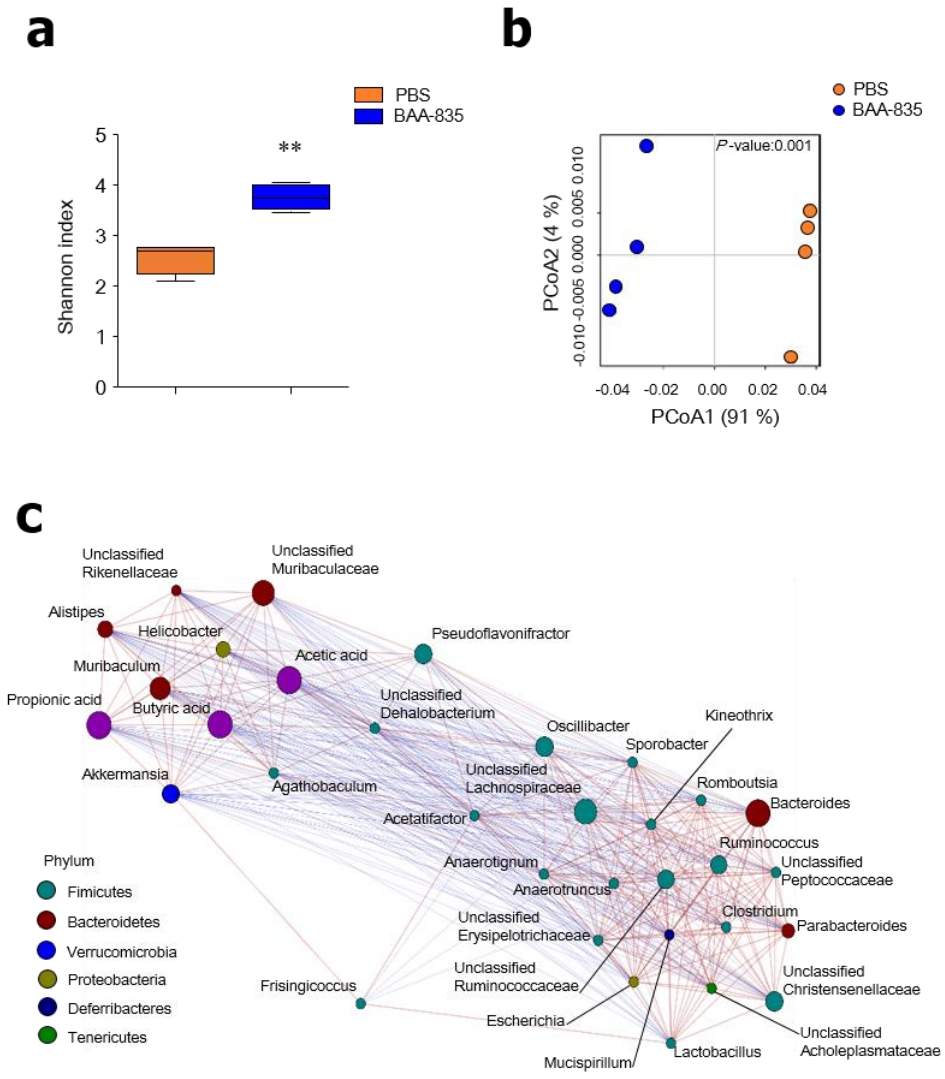

Figure 27. Oral administration of *A. muciniphila* BAA-835 results in change of gut microbiota community. (**a**) Shannon index in fecal microbiome. (**b**) PCoA of weighted Unifrac distances in fecal microbiome. (**c**) Correlation network between SCFAs and fecal microbiome. Dot color represents phylum level. Dot size is proportional to taxon abundance. Statistical analyses were performed by two-tailed paired t-test. n=4. $^{**}p < 0.01$. Data were combined from ≥2 independent experiments.

Oral administration of *A. muciniphila* BAA-835 promotes epithelial differentiation in germ-free mice

To directly address a role of altered gut microbiota, I next adopted germ-free mice and orally administered BAA-835 twice per 2-week interval. Germ-free mice treated with BAA-835 showed increased crypt height and more mucin-producing goblet cells in the SI than did germ-free mice treated with PBS (Figure 28a). In addition, expression levels of *Lgr5*, *Lyz1*, *Muc2*, *Wnt3*, *Axin2*, and *Ctnnb1* in the SI tissues were significantly higher in BAA-835-fed germ-free mice than in PBS-fed germ-free mice (Figure 28b). These results suggest that oral *A. muciniphila* activates epithelial regeneration directly unlike other gut microbiota, which may be altered by *A. muciniphila*.

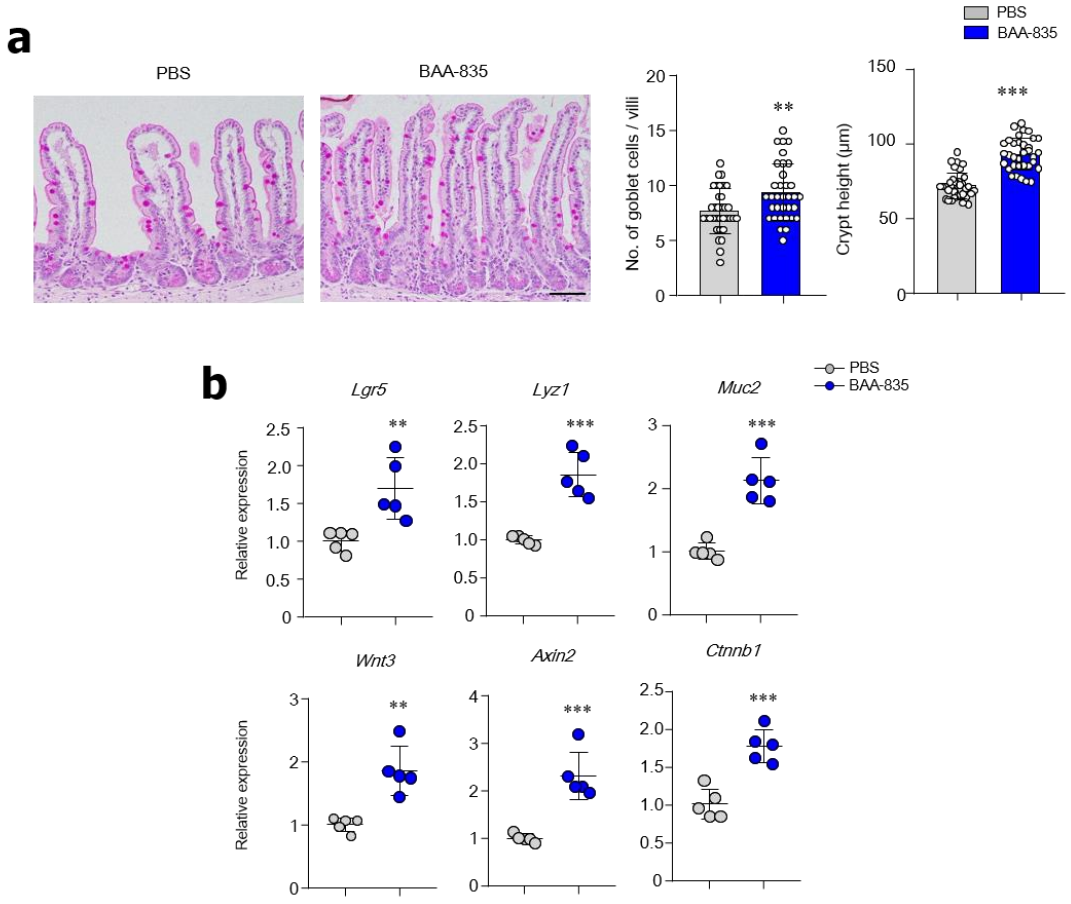

Figure 28. Effectiveness of *A. muciniphila* BAA-835 in germ-free mice. Germ-free mice treated with BAA-835 had enhanced ISC-mediated epithelial development. (**a**) PAS staining of SI and quantification of goblet cell numbers and crypt heights. (**b**) mRNA levels of *Lgr5, Lyz1, Muc2, Wnt3, Axin2,* and *Ctnnb1* in SI tissues. Scale bars: 50 μm (a). Statistical analyses were carried out by two-tailed paired t-test. n=5. $^{**}p < 0.01$, $^{***}p < 0.001$.

Oral administration of *A. muciniphila* BAA-835 repair radiation and chemotherapy gut damage

As *A. muciniphila* promotes ISC-mediated epithelial development, I next investigated whether *A. muciniphila* plays a role in preventing gut damage. Our previous study showed that radiation (R; 10 Gy) and methotrexate (M; MTX) cause severe damage to mouse SI tissues (Lee et al., 2018). In this study, I assessed PBS-treated mice (PBS+R+M) and mice treated with BAA-835 for 4 weeks prior to radiation and MTX treatment (BAA-835+R+M) (Figure 29a). The treated group of mice with *A. muciniphila* had less severe gut damage (Figure 29b). In addition, more numbers of $Lgr5^{+}$ ISCs were maintained in the SI crypt of BAA-835+R+M mice compared with the PBS+R+M mice (Figure 29c). As predicted, BAA-835+R+M mice lost less weight than the PBS+R+M (Figure 29d). The organoid size and number derived from the SI of BAA-835+R+M mice were significantly increased in comparison with those of PBS+R+M-derived SI organoids, indicating that pre-treatment with BAA-835 reduced damage and may play a protective role in the gut (Figure 30). Of note, BAA-835+R+M mice resulted in increased mRNA expression of *Lgr5*, *Lyz1*, *Muc2*, *Wnt3*, *Axin2*, and *Ctnnb1* in the SI tissues compared to PBS+R+M group (Figure 31). These results suggest that the symbiotic actions of *A. muciniphila* may promote gut repair following damage provoked by cancer therapy.

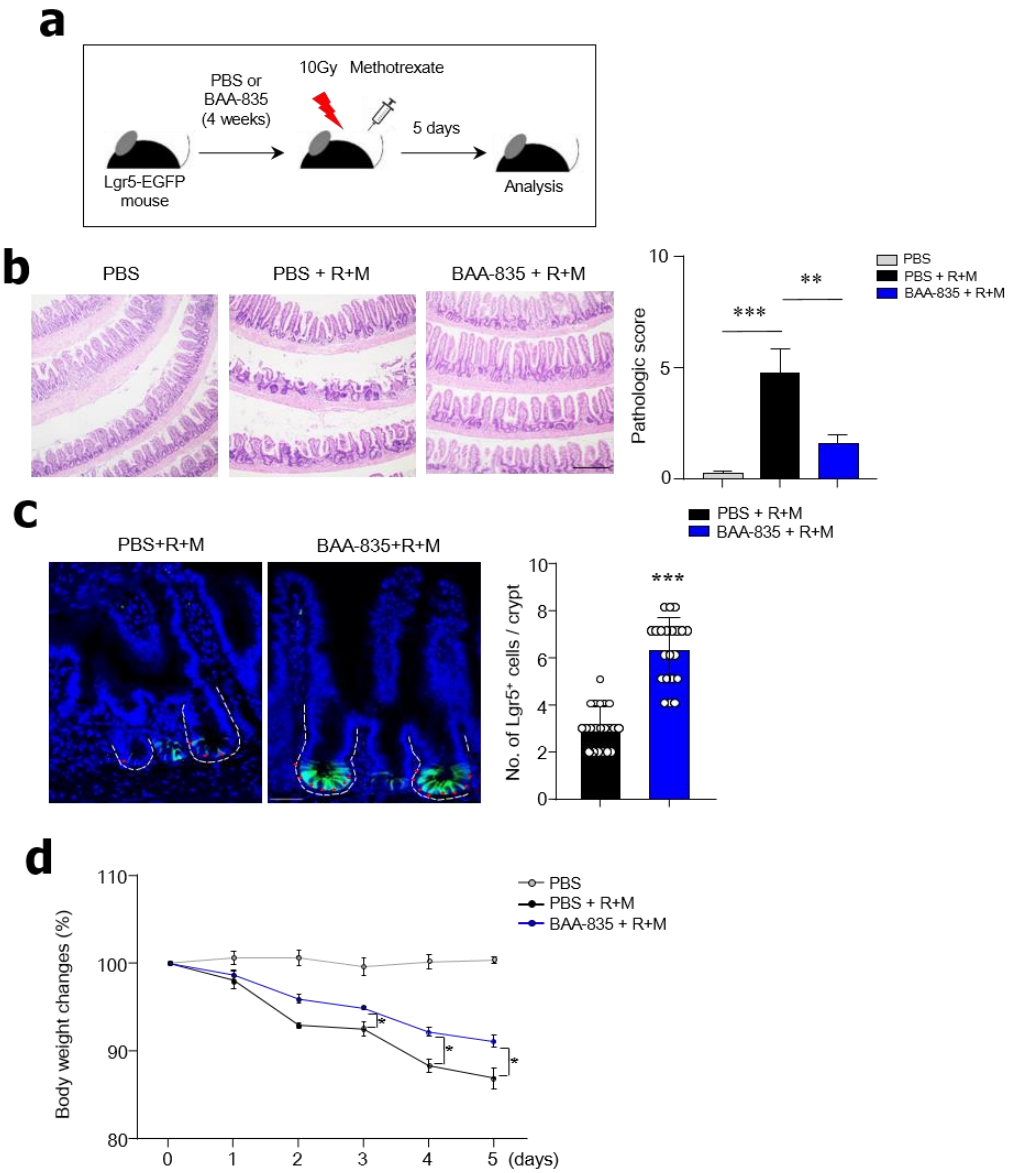

Figure 29. Oral administration of *A. muciniphila* BAA-835 prevents mouse gut injury. (**a**) Timeline of gut injury experiment. (**b**) Pathology and scores of SI by H&E staining. (**c**) Representative confocal image and number of Lgr5 GFP^+ cells in SI following treatment with radiation (R) and methotrexate (M; MTX). (**d**) Body weight changes of mice after treatment with R and MTX. Scale bars: 100 μm (b); 50 μm (c). Statistical analyses were performed by two-tailed paired t-test (c, d) and one-way ANOVA with post hoc Tukey's test (b). n=3. $^{*}p < 0.05$, $^{**}p < 0.01$, $^{***}p < 0.001$. Data were combined from ≥2 independent experiments.

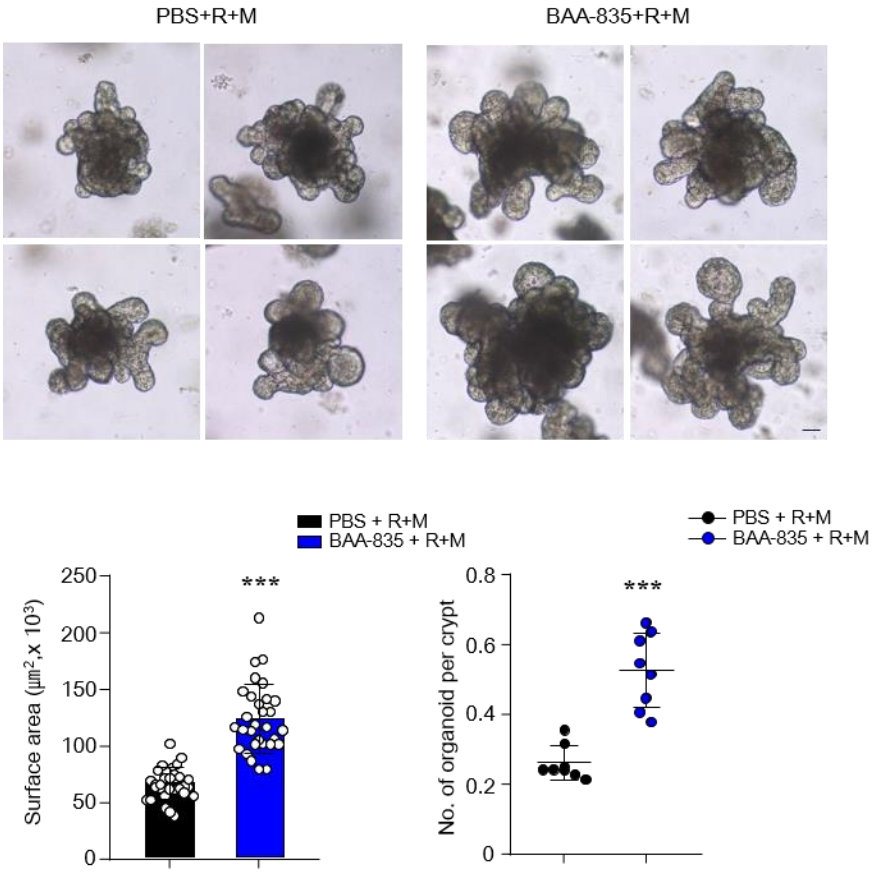

Figure 30. Pre-treatment of *A. muciniphila* BAA-835 increased organogenesis after gut injury. Organoid-forming capacity of SI crypt obtained from mice after treatment with R and MTX. Scale bars: 50 μm. Statistical analyses were performed by two-tailed paired t-test. n=3. $^{*}p < 0.05$, $^{**}p < 0.01$, $^{***}p < 0.001$. Data were combined from ≥2 independent experiments.

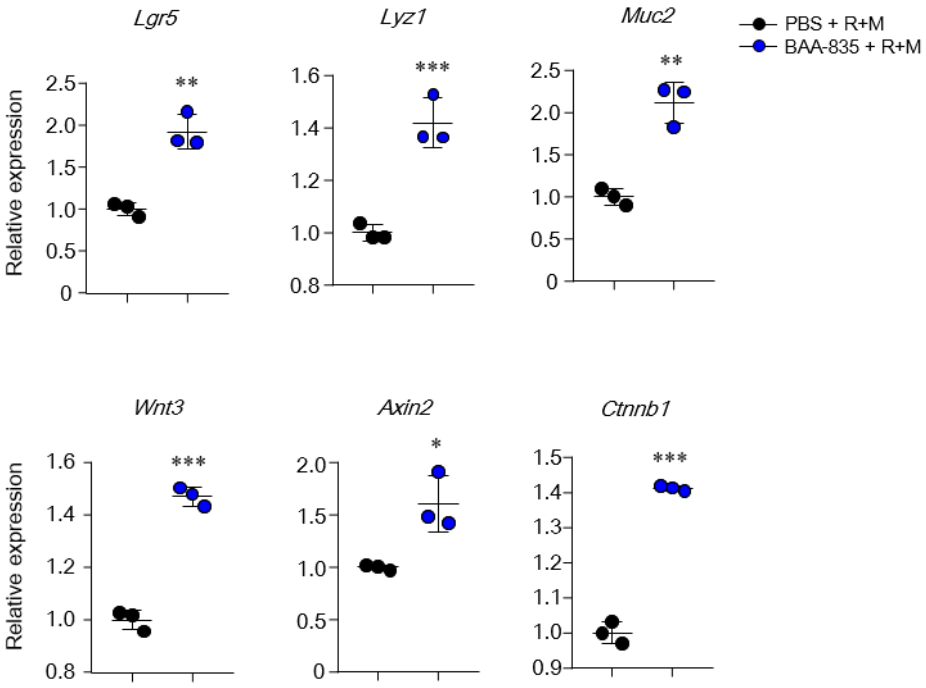

Figure 31. Pre-treatment of *A. muciniphila* BAA-835 increased organogenesis related gene expression after gut injury. mRNA levels of *Lgr5*, *Lyz1*, *Muc2*, *Wnt3*, *Axin2*, and *Ctnnb1* in SI tissues treated R and MTX. Statistical analyses were performed by two-tailed paired t-test. n=3. $^{*}p < 0.05$, $^{**}p < 0.01$, $^{***}p < 0.001$. Data were combined from ≥2 independent experiments.

A. muciniphila AK32 from healthy human feces is superior to BAA-835 for ISC-mediated epithelial development

I next investigated whether an *A. muciniphila* strain isolated from healthy human feces promotes ISC-mediated epithelial development compared with the BAA-835 type strain. By use of selective media and species-specific PCR analysis, I obtained 11 different *A. muciniphila* strains. To evaluate the effect of *A. muciniphila* on ISC-mediated epithelial development, SI-derived organoids were cultured with culture supernatant from one of the strains. Only treatment with the AK32 strain significantly increased organoid size (Figure 32). To address whether increased ISC-mediated epithelial development by the AK32 strain is dependent on SCFAs, the Gpr41/43 antagonist was applied to the cultures. Treatment with the Gpr41/43 antagonist significantly reversed the AK32-mediated effect on SI-derived organoid size (Figure 33). As anticipated, AK32 increased production of acetic acids and propionic acids compared with BAA-835 (Figure 34). To examine how the AK32 enhanced SCFA secretion, the expression levels of two important enzymes, pyruvate dehydrogenase E1 component (Pdh) and Na^+-translocating methylmalonyl-CoA/oxaloacetate decarboxylase (Mmd) were evaluated (Figure 35a). The mRNA expression levels of *pdh* and *mmd* from the AK32 strain were higher than those of the BAA-835 type strain (Figure 35b). Next, I used whole-genome sequencing to analyze the genetic characteristics of AK32. Results shows a complete genome map of the AK32-based Clusters of Orthologous Groups (Figure 36). The trimming information of AK32 was summarized in Table 1. The genomic characteristics (genome size, numbers of coding sequences, and ANIb) of the AK32 strain differed from those of BAA-835 (Table 2). To further determine a novel strain of AK32, I compared the metabolic gallery (API 20A and API ZYM), MALDI-TOF spectrum profiles, growth capacity, and phylogenetic tree. Although AK32 did not differ from BAA-835 in terms of carbohydrate fermentation, AK32 expressed more α-, β-galactosidase than BAA-835 (Figure 37). The matching spectrum with MALDI-TOF MS analysis showed some peaks that differed between AK32 and BAA-835

(Figure 38). The growth capacity of AK32 was identical to BAA-835 at an early stage while CFUs of the AK32 strain after 28 h were downregulated compared to those of BAA-835 (Figure 39). The phylogenetic tree showed the AK32 strain to be closely related to BAA-835 (Figure 40). To further examine *in vivo* function, mice were treated with either AK32 or BAA-835 strains for 4 weeks. Of note, SI organoids from AK32-treated mice were significantly larger than those from mice treated with BAA-835 strain (Figure 41). Administration of AK32 increased SI crypt height and the number of mucin-producing goblet cells compared with SI of mice treated with BAA-835 (Figure 42). Administration of AK32 resulted in increased mRNA expression of *Lgr5*, *Lyz1*, *Muc2*, *Wnt3*, *Axin2*, and *Ctnnb1* in the SI compared with mice treated with BAA-835 (Figure 43). Furthermore, higher levels of acetic and propionic acids were detected in cecal contents of AK32-treated mice than in mice treated with BAA-835 (Figure 44). Thus, I concluded that the newly identified AK32 strain was superior to the BAA-835 type strain in terms of ISC-mediated epithelial development.

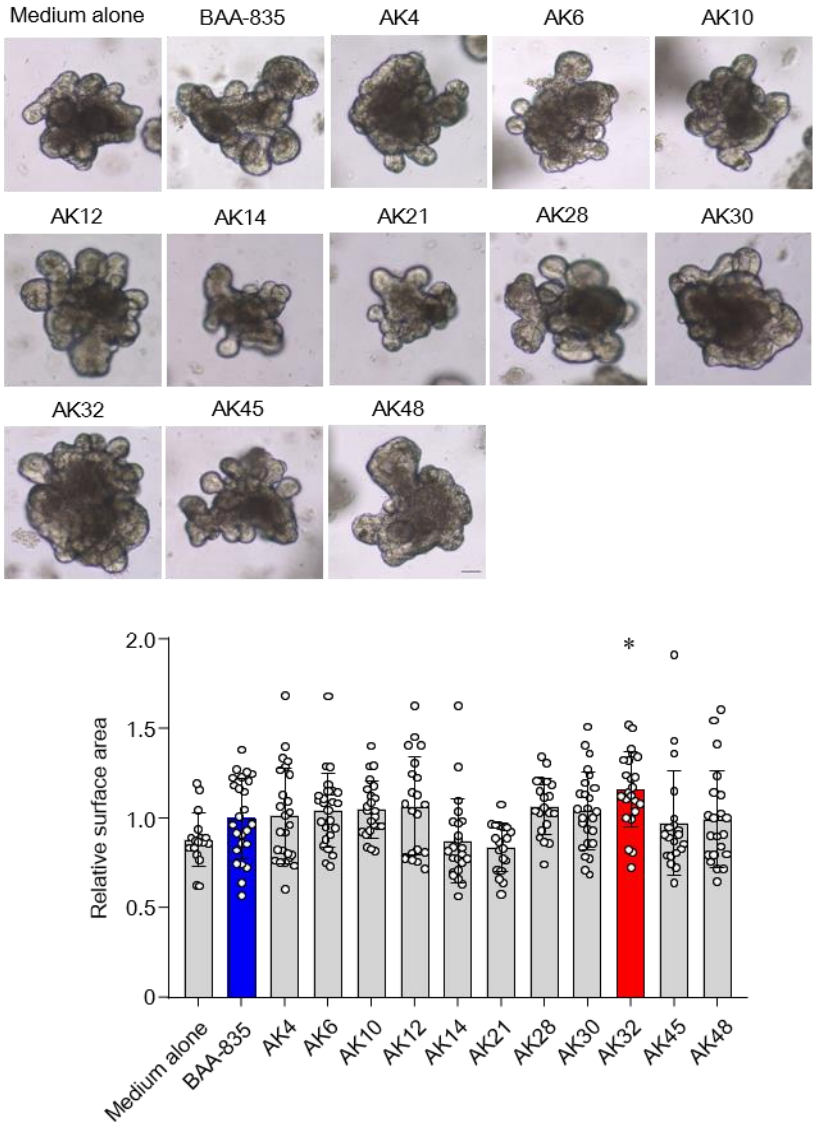

Figure 32. Isolation and validation of new candidates *A. muciniphila* strains. Representative bright-field image and surface area of SI organoids. Treated with culture supernatant from BAA-835 or each 11 *A. muciniphila* isolates. Scale bars: 50 μm. Statistical analyses were performed by one-way ANOVA with post hoc Tukey's test. n=3-5. $^{*}p < 0.05$, $^{**}p < 0.01$, $^{***}p < 0.001$. Data were combined from ≥2 independent experiments.

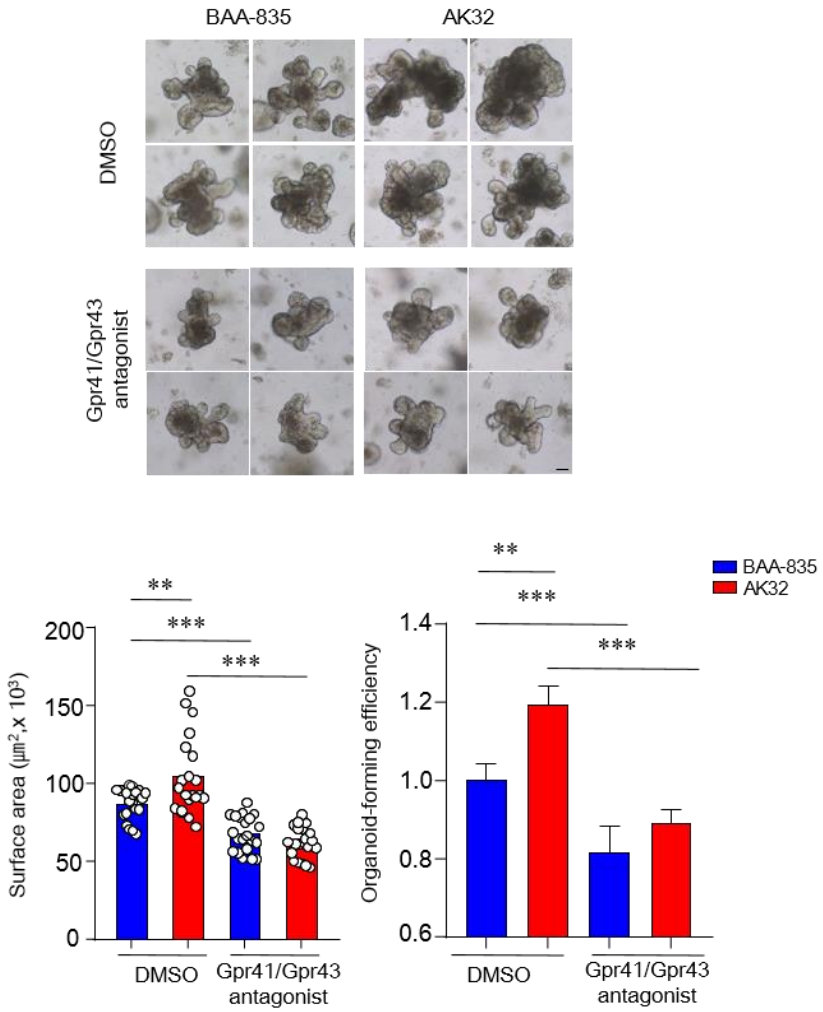

Figure 33. Treatment with Gpr41/43 antagonist reduced SI organogenesis by AK32. Representative bright-field image and surface area of SI organoids. Treated with bacterial culture supernatant in absence or presence of Gpr41/43 antagonists. Scale bars: 50 μm. Statistical analyses were performed by one-way ANOVA with post hoc Tukey's test. n=3-5. $^{**}p < 0.01$, $^{***}p < 0.001$. Data were combined from ≥2 independent experiments.

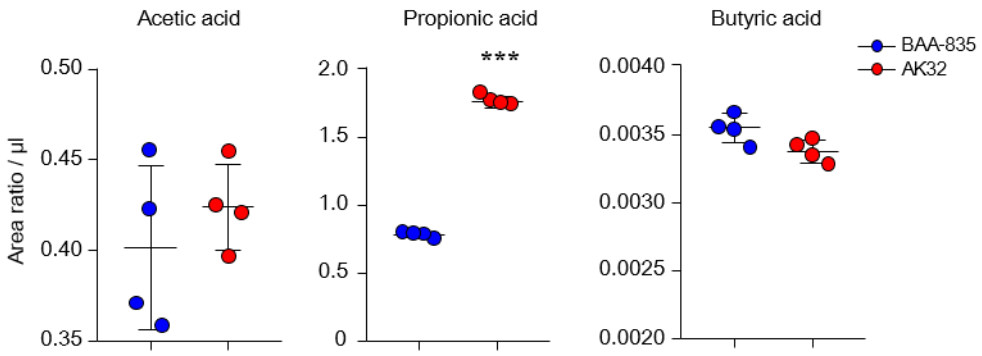

Figure 34. Quantification of SCFA in culture supernatant. Quantification of acetic, propionic, and butyric acids in culture supernatants of *A. muciniphila* BAA-835 or AK32 strain. Statistical analyses were performed by two-tailed paired t-test. $^{***}p < 0.001$.

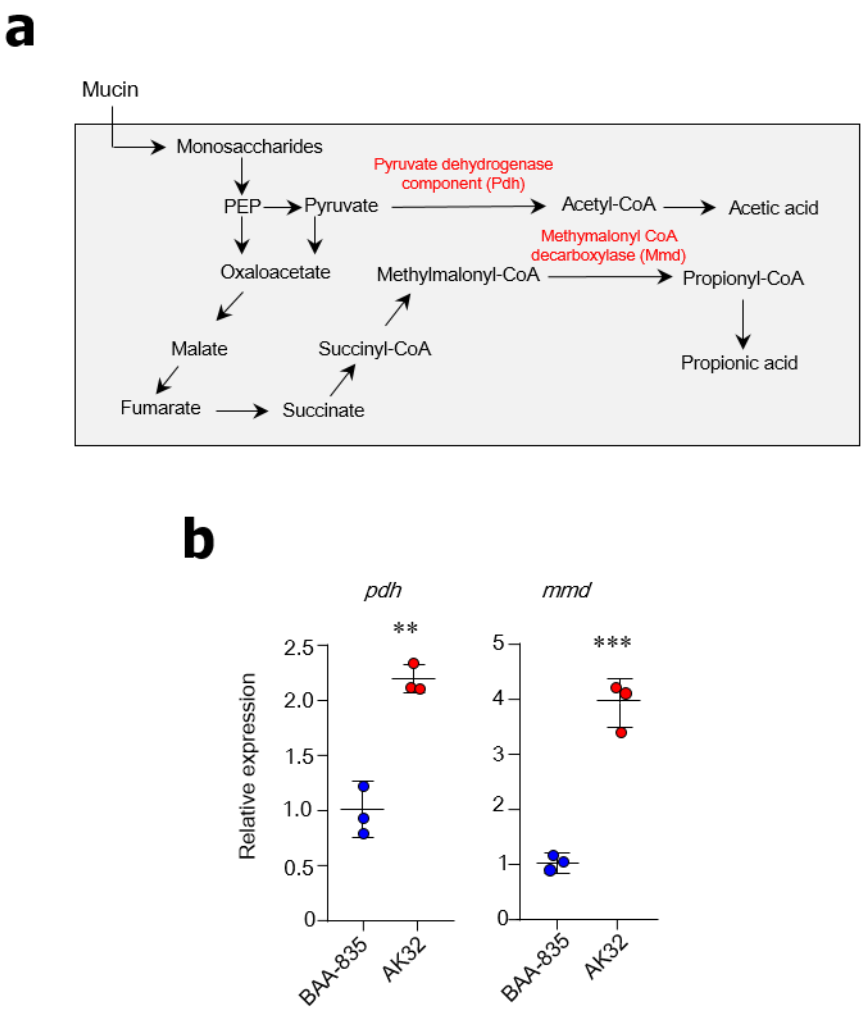

Figure 35. Metabolite pathway and related genes in *A. muciniphila* AK32 strain. (**a**) Model of metabolic pathway for production of acetic and propionic acids. (**b**) mRNA expression levels of pyruvate dehydrogenase E1 component α subunit (*pdh*) and Na^+ transporting methylmalonyl-CoA / oxaloacetate decarboxylase β subunit (*mmd*) in BAA-835 or AK32 strains. Statistical analyses were performed by two-tailed paired t-test. $^{**}p < 0.01$, $^{***}p < 0.001$. Data were combined from ≥2 independent experiments.

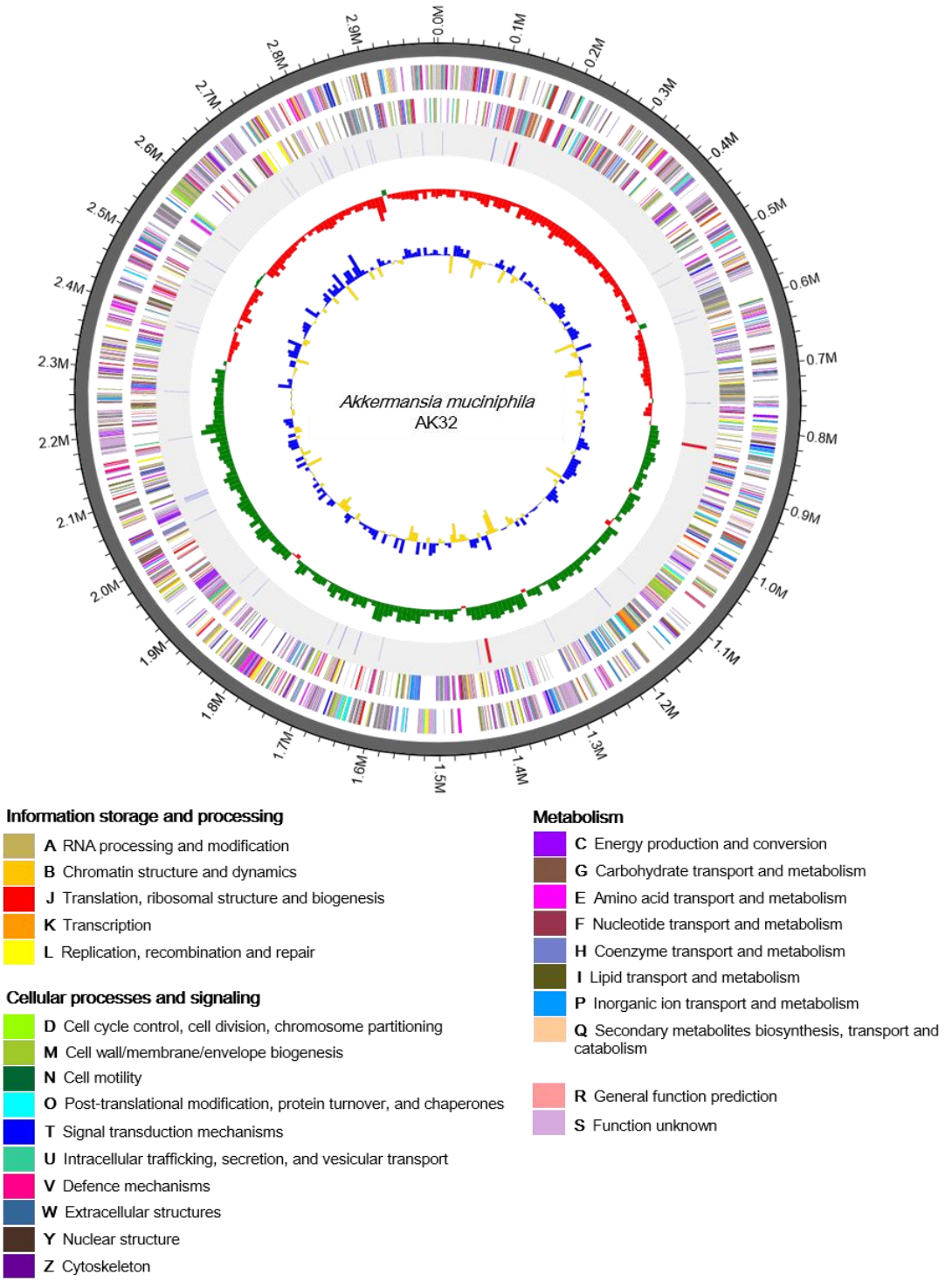

Figure 36. Complete genome map of *A. muciniphila* AK32 strain. All coding sequences were categorized by Clusters of Orthologous Groups (COG) functional categories and colored differently.

Table 1. Summary of trimming information.

	Pre-filter	Post-filter
Polymerase Read Bases	1,038,559,582	990,444,044
Polymerase Reads	150,292	95,828

Table 2. Summary of genome annotation of ATCC BAA-835 and AK32 strains.

Strain	Base (bp)	No. of CDS*	GC contents (%)	tRNA	rRNA	ANIb† (%)
BAA-835	2,664,102	2,184	55.8	53	9	-
AK32	3,004,919	2,600	55.3	56	9	97.39

* Coding sequences

† Average nucleotide identity based BLAST to type strain ATCC BAA-835

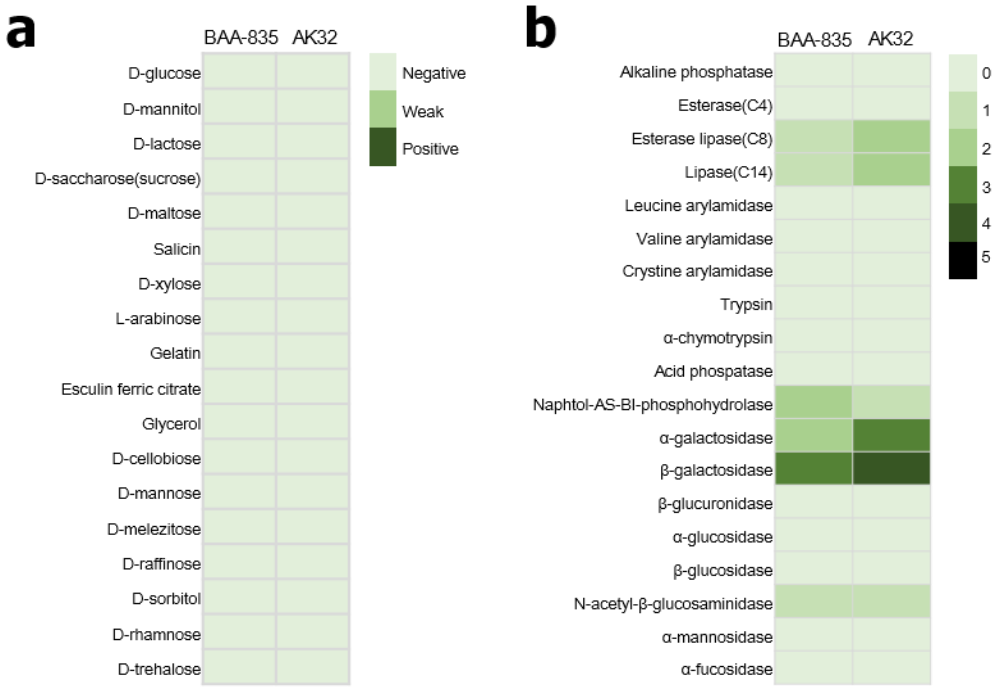

Figure 37. Metabolic gallery of *A. muciniphila* AK32. Profiling of carbohydrate fermentation (**a**) and enzyme activity (**b**) of BAA-835 and AK32 strains.

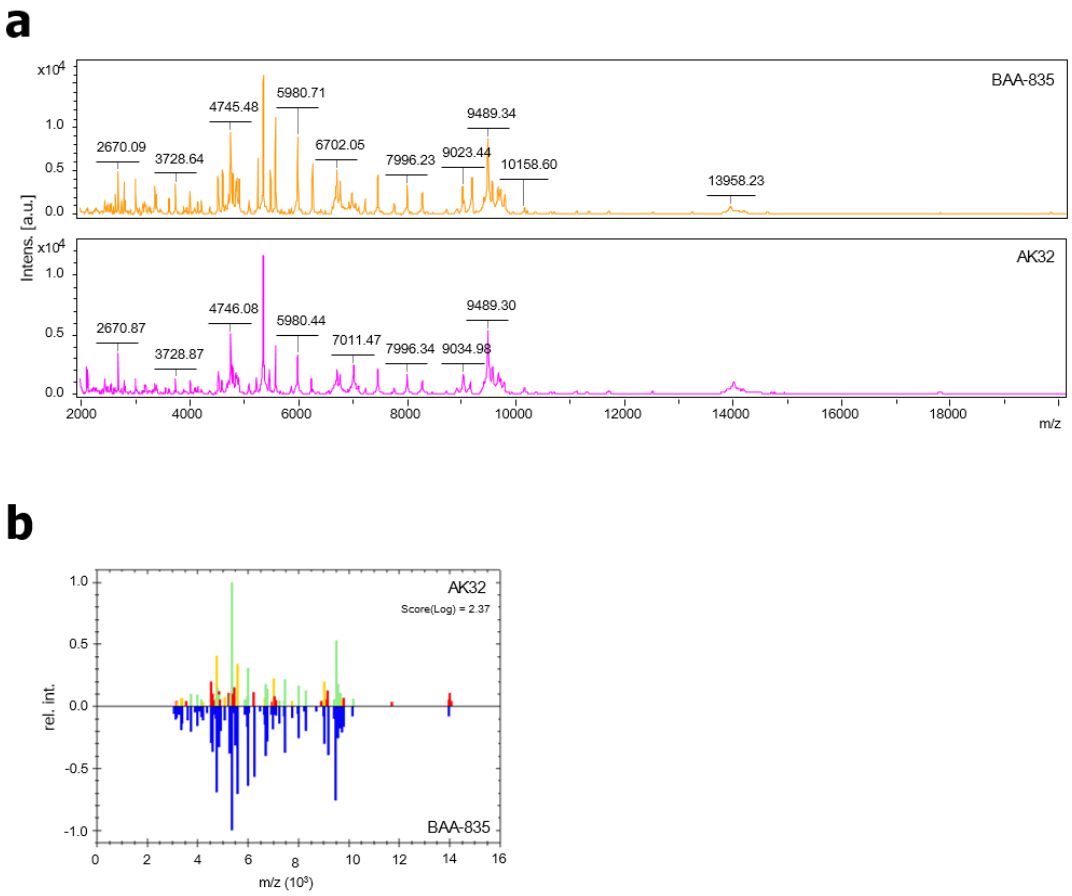

Figure 38. Protein-based characterization of *A. muciniphila* AK32 strain. (**a**) MALDI-TOF MS spectral profiles of *A. muciniphila*. Intens. [a.u]: Intensity [arbitrary unit]. (**b**) Matching spectrum of AK32 against BAA-835. Green: Peak match within experimental error; Yellow: Close peak match, but not within experimental error; Red: No matching peak.

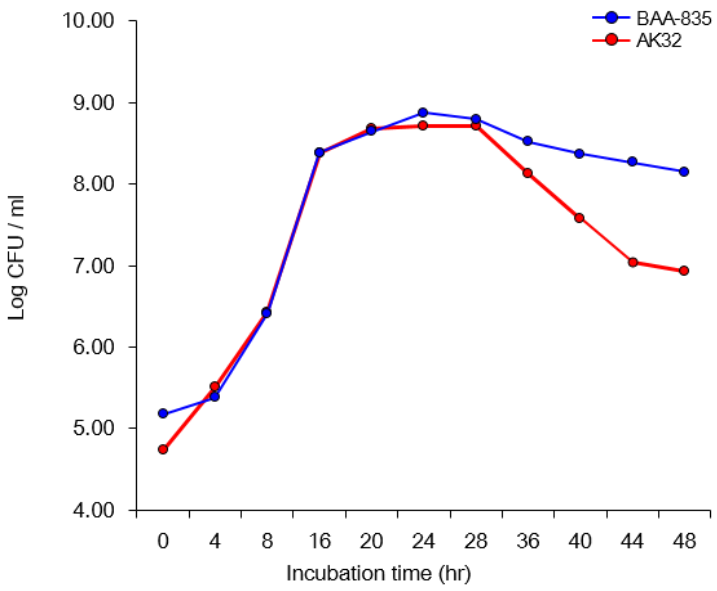

Figure 39. Growth curve of *A. muciniphila* AK32 strain. Comparison study for growth of BAA-835 and AK32 strains.

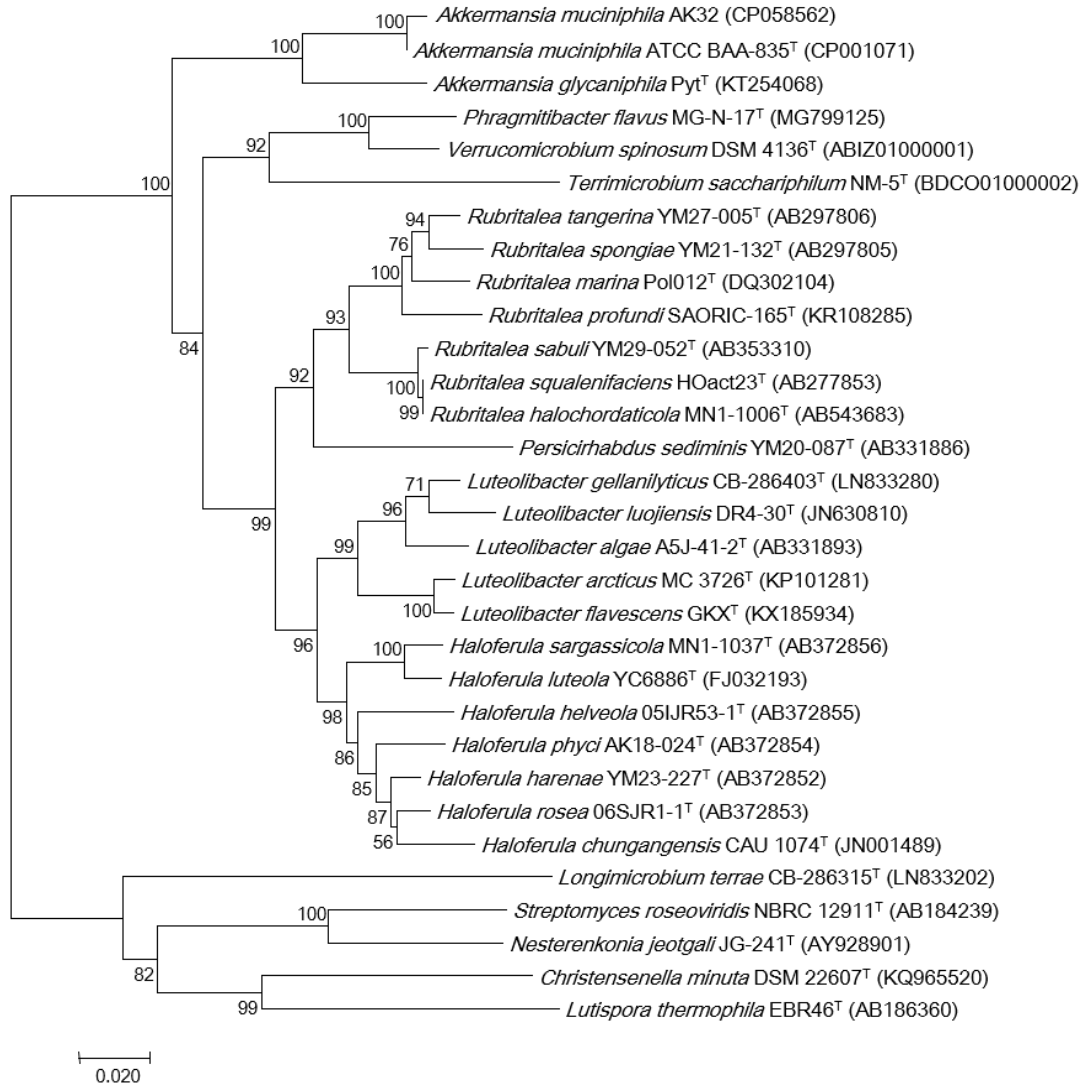

Figure 40. Phylogenetic tree of *A. muciniphila* AK32 strain and related taxa. Phylogenetic tree was inferred using 16S rDNA sequences.

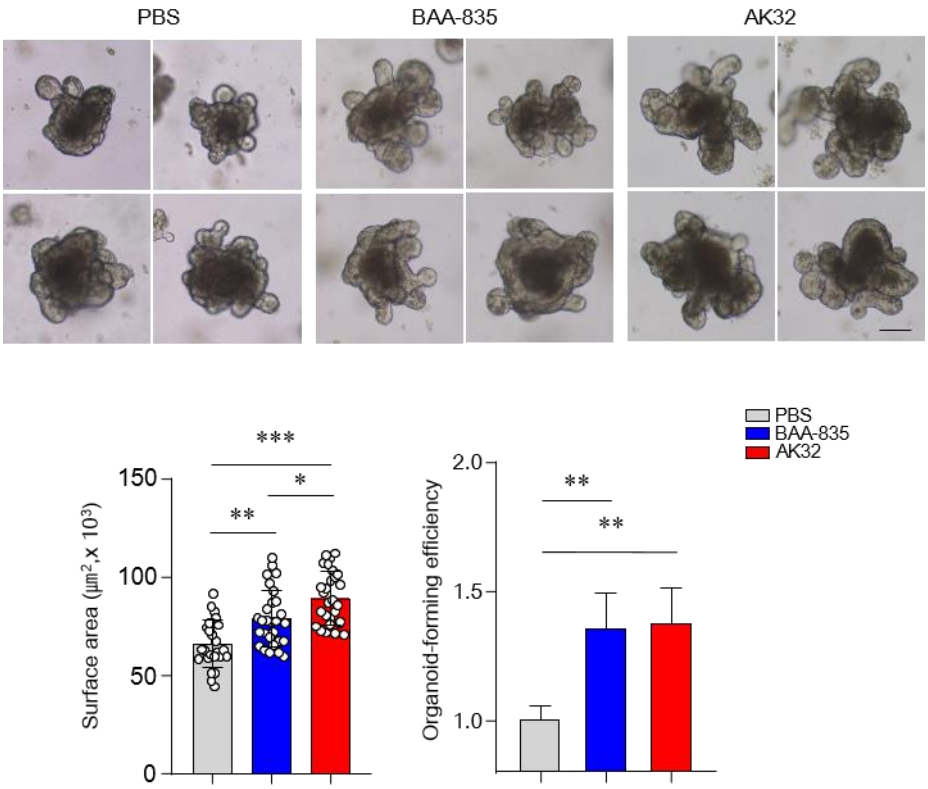

Figure 41. SI organoids from *A. muciniphila* AK32-treated mice showed increased organogenesis. Representative bright-field image, surface area, and forming efficiency of SI-derived organoids from mice treated with PBS or the BAA-835 or AK32 strains. Scale bars: 100 µm. Statistical analyses were performed by one-way ANOVA with post hoc Tukey's test. n=3-5. $^{*}p < 0.05$, $^{**}p < 0.01$, $^{***}p < 0.001$. Data were combined from ≥2 independent experiments.

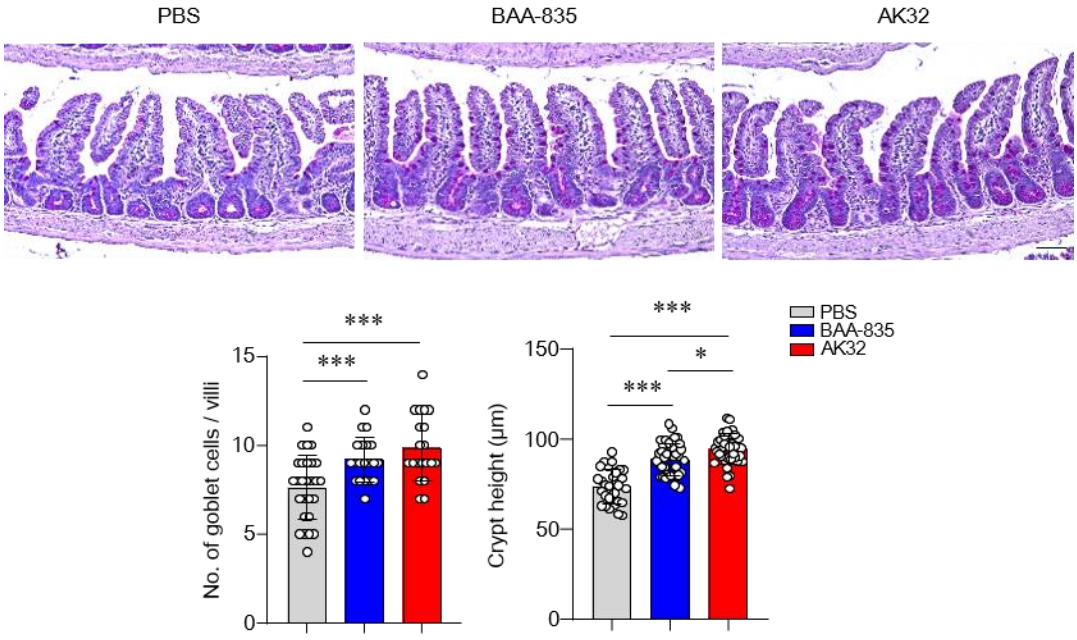

Figure 42. Oral administration with *A. muciniphila* AK32 enhanced epithelial development. Quantification of goblet cells and crypt height in mouse SI. Scale bars: 50 μm. Statistical analyses were performed by one-way ANOVA with post hoc Tukey's test. n=3-5. $^{*}p < 0.05$, $^{**}p < 0.01$, $^{***}p < 0.001$. Data were combined from ≥2 independent experiments.

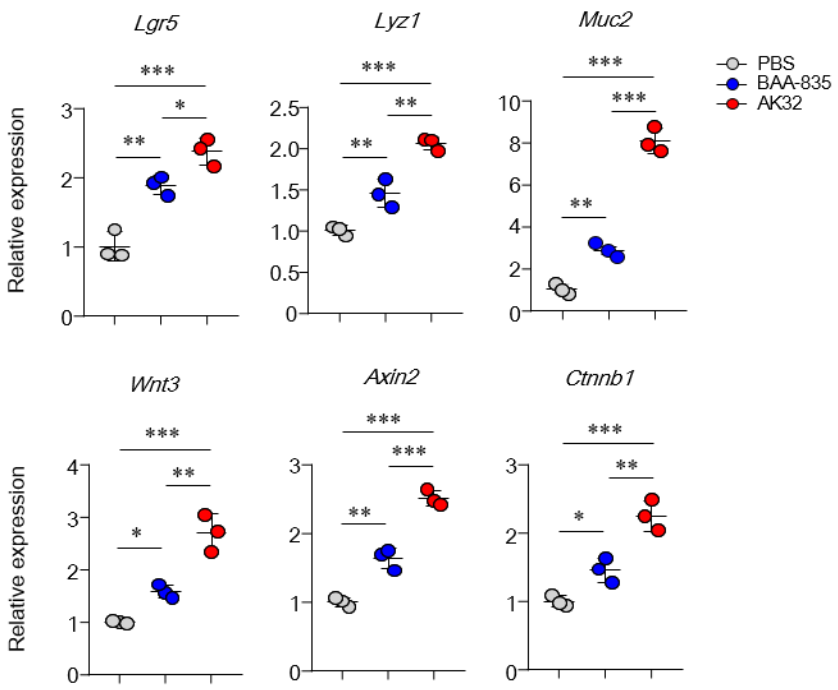

Figure 43. Oral administration with *A. muciniphila* AK32 increased epithelial development related gene expression. mRNA levels of *Lgr5*, *Lyz1*, *Muc2*, *Wnt3*, *Axin2*, and *Ctnnb1* in SI tissues. Statistical analyses were performed by one-way ANOVA with post hoc Tukey's test. n=3-5. $^{*}p < 0.05$, $^{**}p < 0.01$, $^{***}p < 0.001$. Data were combined from ≥2 independent experiments.

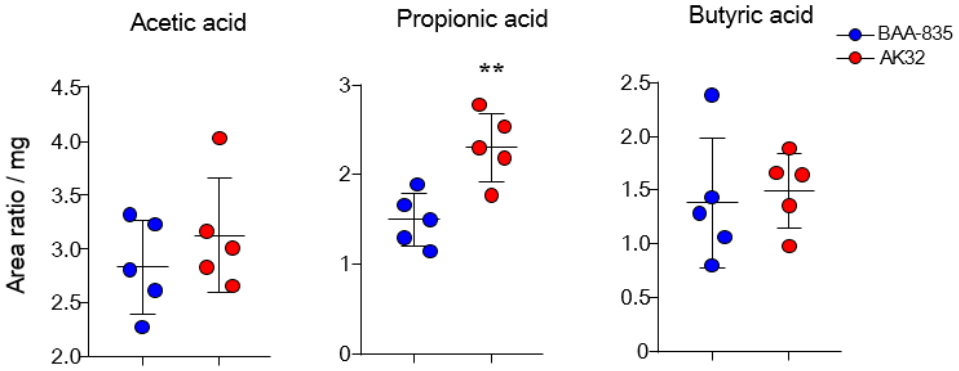

Figure 44. Quantification of SCFA in cecal contents. Quantification of acetic, propionic, and butyric acids in cecal contents of mice treated with BAA-835 or AK32 strains. Statistical analyses were performed by two-tailed paired t-test. $^{**}p < 0.01$.

Discussion

In this study, *A. muciniphila* was found to play a crucial role in ISC-mediated epithelial development by activation of the Wnt signaling pathway and repair of the damaged gut. Treatment with *A. muciniphila* upregulated the expression of genes involved in the Wnt signaling pathway and increased production of SCFA metabolites, such as acetic and propionic acids, which in turn maintain the stemness of ISCs. A novel *A. muciniphila* strain was isolated from healthy human stools that promoted the expression of genes involved in acetic acid and propionic acid production, and therefore may have improved functionality for maintaining gut homeostasis.

The $Lgr5^{+}Ki67^{-}$ cells located at crypt positions +4/+5 of the SI are destined to differentiate into secretory lineage cells (Basak et al., 2014). Administration of *A. muciniphila* resulted in an increased density of $Lgr5^{+}Ki67^{-}$ cells in the SI crypt, which led to an increased number of secretory lineage cells, such as goblet and Paneth cells (Figure 10). The most important pathway for IEC development is Wnt signaling (Korinek et al., 1998; van der Flier and Clevers, 2009). In support of this theory, inhibition of the Wnt pathway was shown to reduce the number of $Math1^{+}$ precursor cells, resulting in a depletion of secretory lineage cells (Pinto et al., 2003). Paneth cells play a critical role in maintaining the ISC niche and the production of Wnt3 (Sato et al., 2011b). In this study, the co-culture of ISCs and Paneth cells demonstrated that Paneth cells from *A. muciniphila*-treated mice directly promoted ISC proliferation in a Wnt3-dependent manner (Figure 18). Thus, I speculate that metabolites produced by *A. muciniphila* stimulate Paneth cells to secrete Wnt3, which then promotes the proliferation of $Lgr5^{+}Ki67^{-}$ cells at SI crypt positions +4/+5.

A previous study reported that *A. muciniphila* uses mucin as an energy source by converting it into acetic and propionic acids (De Vos, 2017). Paradoxically, others have found that *A.*

muciniphila promotes the generation of mucin-secreting goblet cells that were depleted by a high-fat diet (Cani et al., 2013; Everard et al., 2013; Shin et al., 2014). In this study, my aim was to investigate how *A. muciniphila* activates mucin secretion. I propose that acetic and propionic acids produced by *A. muciniphila* may be key factors for supporting the maturation of mucin-secreting goblet cells (Figure 19, 20, and 23).

Another study reported that administration of *A. muciniphila* did not reconstitute the gut microbiome (Depommier et al., 2019). In contrast, I found that *A. muciniphila* altered the gut microbiota composition and structure, which may affect the pattern of metabolite secretion (Figure 26 and 27). Germ-free mice supplemented with *A. muciniphila* had an exacerbated infection by *Salmonella* Typhimurium, suggesting that an over-abundance of *A. muciniphila* diminished microbiome diversity, leading to a deleterious modification of the gut environment (Ganesh et al., 2013). Furthermore, an accumulation of antimicrobial peptide produced by Paneth cells may contribute to a change in gut microbiota (Salzman et al., 2010). I therefore hypothesized that treatment with *A. muciniphila* may alter the bacterial composition and SCFA production in the gut; for example, by altering the abundance of the phyla Bacteroidetes, which produces acetic and propionic acids (Den Besten et al., 2013), or *Alistipes* and *Rikenellaceae*, which produce SCFAs (Martin-Nunez et al., 2019; Rautio et al., 2003). Unexpectedly, however, oral administration of *A. muciniphila* in germ-free mice resulted in enhancement of ISC-mediated epithelial development (Figure 28). Therefore, I conclude there might be two pathways through which *A. muciniphila* increases SCFA production, directly via mucin degradation and indirectly by altering microbiome composition.

Individual bacterial strains, even the same species, have strain-specific abilities. As lactic acid bacterial strains of the same species show different enzymatic activities (Kim et al., 2019), I wondered whether different *A. muciniphila* strains might have varying effects on ISC-mediated epithelial development. I found that the newly identified *A. muciniphila* AK32 strain

activated the expression of genes involved in SCFA production and increased the secretion of acetic and propionic acids (Figure 34 and 35).

Treatment with *A. muciniphila* had a greater effect on the production of propionic acid than on acetic acid. Previously, it was suggested that *A. muciniphila* and propionic acid regulate the expression of genes associated with the host lipid metabolism and activate the epigenome (Lukovac et al., 2014). Accumulating evidence suggests that propionic acid may modulate host physiology in several ways. For example, propionic acid stimulates the release of peptide YY and glucagon-like peptide-1 in human colonic cells, and thereby reduces energy intake and weight gain (Chambers et al., 2015). Intriguingly, propionic acid stimulates Muc2 production by IECs by regulating the expression of the prostaglandins (Willemsen et al., 2003). A recent study proposed that supplementation of propionic acid improves the Treg/Th17 imbalance in multiple sclerosis patients (Duscha et al., 2020). Taken together with my results, I conclude that propionic acid may play an important role in IEC homeostasis and the overall gut, and therefore may modulate host physiology.

Several studies have reported an interaction between gut metabolites and IEC development (Beyaz et al., 2016; Lee et al., 2018). Our prior study revealed that microbiota-derived lactate promotes IEC development (Lee et al., 2018). In contrast, no significant changes in lactate were found in mice treated with *A. muciniphila*, suggesting that lactate is not a crucial metabolite involved in *A. muciniphila*-mediated IEC development (Data not shown). A previous study reported that fatty acids, including palmitic acid, the main metabolite produced by gut microbiota, enhanced ISC proliferation (Beyaz et al., 2016). Furthermore, our recent study demonstrated that dietary cellulose prevented gut inflammation by increasing the *A. muciniphila* population and modulating production of lipid metabolites (Kim et al., 2020). Taken together, *A. muciniphila* treatment may elevate the production of lipid metabolites,

including myristic and palmitic acid, which influence IEC development (Data not shown). Further investigation is warranted to rule out this possibility.

Conclusion

I found that *A. muciniphila* likely plays a crucial role in IEC development and may be a potential clinical therapeutic agent for preventing gut damage. To my knowledge, this is the first study to show the direct effects of *A. muciniphila* on ISC-mediated epithelium development. A new *A. muciniphila* strain was identified from healthy human stools with improved homeostatic functionality, such as increased production of acetic and propionic acids. Furthermore, this study may serve as a valuable basis for identifying and evaluating human microorganisms with therapeutic potential.

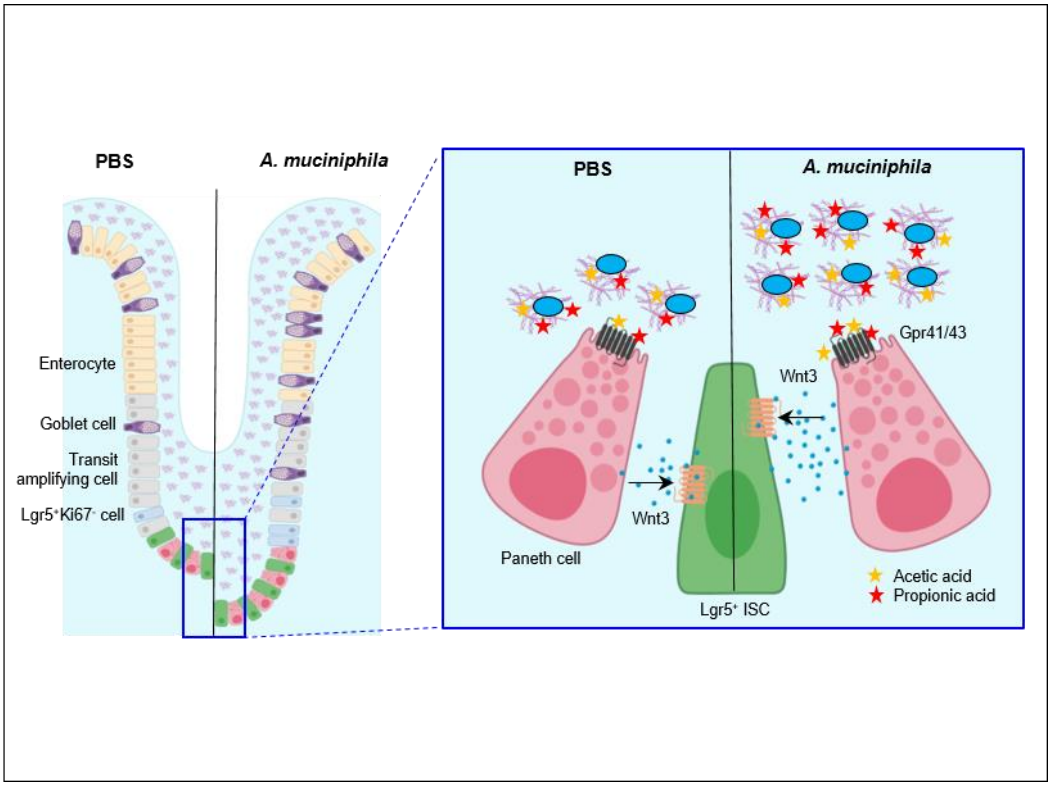

Cross-talk between *A. muciniphila* and IECs controls epithelial development

References

Alam, A., Leoni, G., Quiros, M., Wu, H., Desai, C., Nishio, H., Jones, R.M., Nusrat, A., and Neish, A.S. (2016). The microenvironment of injured murine gut elicits a local pro-restitutive microbiota. Nat Microbiol *1*, 15021.

Barker, N. (2014). Adult intestinal stem cells: critical drivers of epithelial homeostasis and regeneration. Nat Rev Mol Cell Biol *15*, 19-33.

Barker, N., van Es, J.H., Kuipers, J., Kujala, P., van den Born, M., Cozijnsen, M., Haegebarth, A., Korving, J., Begthel, H., Peters, P.J., and Clevers, H. (2007). Identification of stem cells in small intestine and colon by marker gene Lgr5. Nature *449*, 1003-1007.

Basak, O., van de Born, M., Korving, J., Beumer, J., van der Elst, S., van Es, J.H., and Clevers, H. (2014). Mapping early fate determination in Lgr5+ crypt stem cells using a novel Ki67-RFP allele. EMBO J *33*, 2057-2068.

Behrens, J., von Kries, J.P., Kuhl, M., Bruhn, L., Wedlich, D., Grosschedl, R., and Birchmeier, W. (1996). Functional interaction of beta-catenin with the transcription factor LEF-1. Nature *382*, 638-642.

Belkaid, Y., and Hand, T.W. (2014). Role of the microbiota in immunity and inflammation. Cell *157*, 121-141.

Beyaz, S., Mana, M.D., Roper, J., Kedrin, D., Saadatpour, A., Hong, S.J., Bauer-Rowe, K.E., Xifaras, M.E., Akkad, A., Arias, E.*, et al.* (2016). High-fat diet enhances stemness and tumorigenicity of intestinal progenitors. Nature *531*, 53-58.

Bjerknes, M., and Cheng, H. (1999). Clonal analysis of mouse intestinal epithelial progenitors. Gastroenterology *116*, 7-14.

Cani, P.D., and de Vos, W.M. (2017). Next-Generation Beneficial Microbes: The Case of Akkermansia muciniphila. Front Microbiol *8*, 1765.

Cani, P.D., Everard, A., and Duparc, T. (2013). Gut microbiota, enteroendocrine functions and metabolism. Curr Opin Pharmacol *13*, 935-940.

Chambers, E.S., Viardot, A., Psichas, A., Morrison, D.J., Murphy, K.G., Zac-Varghese, S.E., MacDougall, K., Preston, T., Tedford, C., Finlayson, G.S.*, et al.* (2015). Effects of targeted

delivery of propionate to the human colon on appetite regulation, body weight maintenance and adiposity in overweight adults. Gut *64*, 1744-1754.

Chevalier, C., Stojanovic, O., Colin, D.J., Suarez-Zamorano, N., Tarallo, V., Veyrat-Durebex, C., Rigo, D., Fabbiano, S., Stevanovic, A., Hagemann, S.*, et al.* (2015). Gut Microbiota Orchestrates Energy Homeostasis during Cold. Cell *163*, 1360-1374.

Clevers, H. (2013). The intestinal crypt, a prototype stem cell compartment. Cell *154*, 274-284.

De Vos, W.M. (2017). Microbe Profile: Akkermansia muciniphila: a conserved intestinal symbiont that acts as the gatekeeper of our mucosa. Microbiology *163*, 646-648.

Den Besten, G., van Eunen, K., Groen, A.K., Venema, K., Reijngoud, D.J., and Bakker, B.M. (2013). The role of short-chain fatty acids in the interplay between diet, gut microbiota, and host energy metabolism. J Lipid Res *54*, 2325-2340.

Depommier, C., Everard, A., Druart, C., Plovier, H., Van Hul, M., Vieira-Silva, S., Falony, G., Raes, J., Maiter, D., Delzenne, N.M.*, et al.* (2019). Supplementation with Akkermansia muciniphila in overweight and obese human volunteers: a proof-of-concept exploratory study. Nat Med *25*, 1096-1103.

Derrien, M., Collado, M.C., Ben-Amor, K., Salminen, S., and de Vos, W.M. (2008). The Mucin degrader Akkermansia muciniphila is an abundant resident of the human intestinal tract. Appl Environ Microbiol *74*, 1646-1648.

Derrien, M., Vaughan, E.E., Plugge, C.M., and de Vos, W.M. (2004). Akkermansia muciniphila gen. nov., sp. nov., a human intestinal mucin-degrading bacterium. Int J Syst Evol Microbiol *54*, 1469-1476.

Duscha, A., Gisevius, B., Hirschberg, S., Yissachar, N., Stangl, G.I., Eilers, E., Bader, V., Haase, S., Kaisler, J., David, C.*, et al.* (2020). Propionic Acid Shapes the Multiple Sclerosis Disease Course by an Immunomodulatory Mechanism. Cell *180*, 1067-1080 e1016.

Everard, A., Belzer, C., Geurts, L., Ouwerkerk, J.P., Druart, C., Bindels, L.B., Guiot, Y., Derrien, M., Muccioli, G.G., Delzenne, N.M.*, et al.* (2013). Cross-talk between Akkermansia muciniphila and intestinal epithelium controls diet-induced obesity. Proc Natl Acad Sci U S A *110*, 9066-9071.

Farin, H.F., Van Es, J.H., and Clevers, H. (2012). Redundant sources of Wnt regulate intestinal stem cells and promote formation of Paneth cells. Gastroenterology *143*, 1518-1529 e1517.

Furusawa, Y., Obata, Y., Fukuda, S., Endo, T.A., Nakato, G., Takahashi, D., Nakanishi, Y., Uetake, C., Kato, K., Kato, T.*, et al.* (2013). Commensal microbe-derived butyrate induces the differentiation of colonic regulatory T cells. Nature *504*, 446-450.

Ganesh, B.P., Klopfleisch, R., Loh, G., and Blaut, M. (2013). Commensal Akkermansia muciniphila exacerbates gut inflammation in Salmonella Typhimurium-infected gnotobiotic mice. PLoS One *8*, e74963.

Gregorieff, A., Stange, D.E., Kujala, P., Begthel, H., van den Born, M., Korving, J., Peters, P.J., and Clevers, H. (2009). The ets-domain transcription factor Spdef promotes maturation of goblet and paneth cells in the intestinal epithelium. Gastroenterology *137*, 1333-1345 e1331-1333.

Human Microbiome Project, C. (2012). Structure, function and diversity of the healthy human microbiome. Nature *486*, 207-214.

Hyatt, D., Chen, G.L., Locascio, P.F., Land, M.L., Larimer, F.W., and Hauser, L.J. (2010). Prodigal: prokaryotic gene recognition and translation initiation site identification. BMC Bioinformatics *11*, 119.

Ireland, H., Kemp, R., Houghton, C., Howard, L., Clarke, A.R., Sansom, O.J., and Winton, D.J. (2004). Inducible Cre-mediated control of gene expression in the murine gastrointestinal tract: effect of loss of beta-catenin. Gastroenterology *126*, 1236-1246.

Kim, J.H., Doo, E.H., Jeong, M., Kim, S., Lee, Y.Y., Yang, J., Lee, J.S., Kim, J.H., Lee, K.W., Huh, C.S., and Byun, S. (2019). Enhancing Immunomodulatory Function of Red Ginseng Through Fermentation Using Bifidobacterium animalis Subsp. lactis LT 19-2. Nutrients *11*.

Kim, Y., Hwang, S.W., Kim, S., Lee, Y.S., Kim, T.Y., Lee, S.H., Kim, S.J., Yoo, H.J., Kim, E.N., and Kweon, M.N. (2020). Dietary cellulose prevents gut inflammation by modulating lipid metabolism and gut microbiota. Gut Microbes, 1-18.

Koeth, R.A., Wang, Z., Levison, B.S., Buffa, J.A., Org, E., Sheehy, B.T., Britt, E.B., Fu, X., Wu, Y., Li, L.*, et al.* (2013). Intestinal microbiota metabolism of L-carnitine, a nutrient in red meat, promotes atherosclerosis. Nat Med *19*, 576-585.

Korinek, V., Barker, N., Moerer, P., van Donselaar, E., Huls, G., Peters, P.J., and Clevers, H. (1998). Depletion of epithelial stem-cell compartments in the small intestine of mice lacking Tcf-4. Nat Genet *19*, 379-383.

Lee, H., and Ko, G. (2014). Effect of metformin on metabolic improvement and gut microbiota. Appl Environ Microbiol *80*, 5935-5943.

Lee, Y.S., Kim, T.Y., Kim, Y., Lee, S.H., Kim, S., Kang, S.W., Yang, J.Y., Baek, I.J., Sung, Y.H., Park, Y.Y.*, et al.* (2018). Microbiota-Derived Lactate Accelerates Intestinal Stem-Cell-Mediated Epithelial Development. Cell Host Microbe *24*, 833-846 e836.

Lukovac, S., Belzer, C., Pellis, L., Keijser, B.J., de Vos, W.M., Montijn, R.C., and Roeselers, G. (2014). Differential modulation by Akkermansia muciniphila and Faecalibacterium prausnitzii of host peripheral lipid metabolism and histone acetylation in mouse gut organoids. mBio *5*.

Macia, L., Tan, J., Vieira, A.T., Leach, K., Stanley, D., Luong, S., Maruya, M., Ian McKenzie, C., Hijikata, A., Wong, C.*, et al.* (2015). Metabolite-sensing receptors GPR43 and GPR109A facilitate dietary fibre-induced gut homeostasis through regulation of the inflammasome. Nat Commun *6*, 6734.

Martin-Nunez, G.M., Cornejo-Pareja, I., Coin-Araguez, L., Roca-Rodriguez, M.D.M., Munoz-Garach, A., Clemente-Postigo, M., Cardona, F., Moreno-Indias, I., and Tinahones, F.J. (2019). H. pylori eradication with antibiotic treatment causes changes in glucose homeostasis related to modifications in the gut microbiota. PLoS One *14*, e0213548.

Maslowski, K.M., Vieira, A.T., Ng, A., Kranich, J., Sierro, F., Yu, D., Schilter, H.C., Rolph, M.S., Mackay, F., Artis, D.*, et al.* (2009). Regulation of inflammatory responses by gut microbiota and chemoattractant receptor GPR43. Nature *461*, 1282-1286.

Mazmanian, S.K., Round, J.L., and Kasper, D.L. (2008). A microbial symbiosis factor prevents intestinal inflammatory disease. Nature *453*, 620-625.

Miller, T.L., and Wolin, M.J. (1996). Pathways of acetate, propionate, and butyrate formation by the human fecal microbial flora. Appl Environ Microbiol *62*, 1589-1592.

Nawrocki, E.P., and Eddy, S.R. (2013). Infernal 1.1: 100-fold faster RNA homology searches. Bioinformatics *29*, 2933-2935.

Pinto, D., Gregorieff, A., Begthel, H., and Clevers, H. (2003). Canonical Wnt signals are essential for homeostasis of the intestinal epithelium. Genes Dev *17*, 1709-1713.

Plovier, H., Everard, A., Druart, C., Depommier, C., Van Hul, M., Geurts, L., Chilloux, J., Ottman, N., Duparc, T., Lichtenstein, L.*, et al.* (2017). A purified membrane protein from Akkermansia muciniphila or the pasteurized bacterium improves metabolism in obese and diabetic mice. Nat Med *23*, 107-113.

Png, C.W., Linden, S.K., Gilshenan, K.S., Zoetendal, E.G., McSweeney, C.S., Sly, L.I., McGuckin, M.A., and Florin, T.H. (2010). Mucolytic bacteria with increased prevalence in IBD mucosa augment in vitro utilization of mucin by other bacteria. Am J Gastroenterol *105*, 2420-2428.

Rautio, M., Eerola, E., Vaisanen-Tunkelrott, M.L., Molitoris, D., Lawson, P., Collins, M.D., and Jousimies-Somer, H. (2003). Reclassification of Bacteroides putredinis (Weinberg et al., 1937) in a new genus Alistipes gen. nov., as Alistipes putredinis comb. nov., and description of Alistipes finegoldii sp. nov., from human sources. Syst Appl Microbiol *26*, 182-188.

Routy, B., Le Chatelier, E., Derosa, L., Duong, C.P.M., Alou, M.T., Daillere, R., Fluckiger, A., Messaoudene, M., Rauber, C., Roberti, M.P.*, et al.* (2018). Gut microbiome influences efficacy of PD-1-based immunotherapy against epithelial tumors. Science *359*, 91-97.

Salzman, N.H., Hung, K., Haribhai, D., Chu, H., Karlsson-Sjoberg, J., Amir, E., Teggatz, P., Barman, M., Hayward, M., Eastwood, D.*, et al.* (2010). Enteric defensins are essential regulators of intestinal microbial ecology. Nat Immunol *11*, 76-83.

Sato, T., Stange, D.E., Ferrante, M., Vries, R.G., Van Es, J.H., Van den Brink, S., Van Houdt, W.J., Pronk, A., Van Gorp, J., Siersema, P.D., and Clevers, H. (2011a). Long-term expansion of epithelial organoids from human colon, adenoma, adenocarcinoma, and Barrett's epithelium. Gastroenterology *141*, 1762-1772.

Sato, T., van Es, J.H., Snippert, H.J., Stange, D.E., Vries, R.G., van den Born, M., Barker, N., Shroyer, N.F., van de Wetering, M., and Clevers, H. (2011b). Paneth cells constitute the niche for Lgr5 stem cells in intestinal crypts. Nature *469*, 415-418.

Sato, T., Vries, R.G., Snippert, H.J., van de Wetering, M., Barker, N., Stange, D.E., van Es, J.H., Abo, A., Kujala, P., Peters, P.J., and Clevers, H. (2009). Single Lgr5 stem cells build crypt-villus structures in vitro without a mesenchymal niche. Nature *459*, 262-265.

Schattner, P., Brooks, A.N., and Lowe, T.M. (2005). The tRNAscan-SE, snoscan and snoGPS web servers for the detection of tRNAs and snoRNAs. Nucleic Acids Res *33*, W686-689.

Schneeberger, M., Everard, A., Gomez-Valades, A.G., Matamoros, S., Ramirez, S., Delzenne, N.M., Gomis, R., Claret, M., and Cani, P.D. (2015). Akkermansia muciniphila inversely correlates with the onset of inflammation, altered adipose tissue metabolism and metabolic disorders during obesity in mice. Sci Rep *5*, 16643.

Segata, N., Izard, J., Waldron, L., Gevers, D., Miropolsky, L., Garrett, W.S., and Huttenhower, C. (2011). Metagenomic biomarker discovery and explanation. Genome Biol *12*, R60.

Shin, N.R., Lee, J.C., Lee, H.Y., Kim, M.S., Whon, T.W., Lee, M.S., and Bae, J.W. (2014). An increase in the Akkermansia spp. population induced by metformin treatment improves glucose homeostasis in diet-induced obese mice. Gut *63*, 727-735.

Skelly, A.N., Sato, Y., Kearney, S., and Honda, K. (2019). Mining the microbiota for microbial and metabolite-based immunotherapies. Nat Rev Immunol *19*, 305-323.

Turnbaugh, P.J., Ley, R.E., Mahowald, M.A., Magrini, V., Mardis, E.R., and Gordon, J.I. (2006). An obesity-associated gut microbiome with increased capacity for energy harvest. Nature *444*, 1027-1031.

Valles-Colomer, M., Falony, G., Darzi, Y., Tigchelaar, E.F., Wang, J., Tito, R.Y., Schiweck, C., Kurilshikov, A., Joossens, M., Wijmenga, C.*, et al.* (2019). The neuroactive potential of the human gut microbiota in quality of life and depression. Nat Microbiol *4*, 623-632.

van de Wetering, M., Sancho, E., Verweij, C., de Lau, W., Oving, I., Hurlstone, A., van der Horn, K., Batlle, E., Coudreuse, D., Haramis, A.P.*, et al.* (2002). The beta-catenin/TCF-4 complex imposes a crypt progenitor phenotype on colorectal cancer cells. Cell *111*, 241-250.

van der Flier, L.G., and Clevers, H. (2009). Stem cells, self-renewal, and differentiation in the intestinal epithelium. Annu Rev Physiol *71*, 241-260.

van Es, J.H., Sato, T., van de Wetering, M., Lyubimova, A., Yee Nee, A.N., Gregorieff, A., Sasaki, N., Zeinstra, L., van den Born, M., Korving, J.*, et al.* (2012). Dll1+ secretory progenitor cells revert to stem cells upon crypt damage. Nat Cell Biol *14*, 1099-1104.

Willemsen, L.E., Koetsier, M.A., van Deventer, S.J., and van Tol, E.A. (2003). Short chain fatty acids stimulate epithelial mucin 2 expression through differential effects on prostaglandin E(1) and E(2) production by intestinal myofibroblasts. Gut *52*, 1442-1447.

Wong, V.W., Stange, D.E., Page, M.E., Buczacki, S., Wabik, A., Itami, S., van de Wetering, M., Poulsom, R., Wright, N.A., Trotter, M.W*., et al.* (2012). Lrig1 controls intestinal stem-cell homeostasis by negative regulation of ErbB signalling. Nat Cell Biol *14*, 401-408.

Xu, J., and Gordon, J.I. (2003). Honor thy symbionts. Proc Natl Acad Sci U S A *100*, 10452-10459.

Yang, Q., Bermingham, N.A., Finegold, M.J., and Zoghbi, H.Y. (2001). Requirement of Math1 for secretory cell lineage commitment in the mouse intestine. Science *294*, 2155-2158.

Yoon, S.H., Ha, S.M., Kwon, S., Lim, J., Kim, Y., Seo, H., and Chun, J. (2017). Introducing EzBioCloud: a taxonomically united database of 16S rRNA gene sequences and whole-genome assemblies. Int J Syst Evol Microbiol *67*, 1613-1617.

Zakrzewski, M., Proietti, C., Ellis, J.J., Hasan, S., Brion, M.J., Berger, B., and Krause, L. (2017). Calypso: a user-friendly web-server for mining and visualizing microbiome-environment interactions. Bioinformatics *33*, 782-783.

국문 요약

뮤신 분해 균은 장 상피세포 근처에 밀집하여 있다고 알려져 있지만, 그 둘 간의 상호작용에 대하여는 명확하게 규명되어진 바가 없다. 뮤신 분해 균이 어떻게 장내 항상성 조절에 기여하는지 규명하기 위해, 대표적인 뮤신 분해 균으로 알려진 *Akkermansia muciniphila* 균을 마우스에 투여하였다. *A. muciniphila* 투여 4 주 후에 소장에 있는 $Lgr5^{+}$장 줄기세포의 증식이 증가하였음을 확인하였다. 또한 파네스 세포, 술잔세포로의 분화도 촉진되었음을 확인하였다. 대장에서 또한 유사한 효과를 확인하였다. *A. muciniphila* 를 투여한 마우스의 맹장에서 아세트산과 프로피오산의 농도가 PBS 투여 마우스 보다 높은 것을 확인하였다. *A. muciniphila* 를 투여한 마우스 유래의 맹장 내용물을 소장 오가노이드에 처리하였고, 오가노이드의 크기가 증가함을 확인하였다. 이러한 효과는 Gpr41/43 길항제를 처리하였을 때 감소하였다. *A. muciniphila* 를 마우스에 미리 투여하였을 때, 방사선과 Methotrexate 에 의한 장 손상이 감소함을 확인하였다. 건강인 분변 유래의 신규한 *A. muciniphila* 를 분리하였고, 이 균주는 기준 균주보다 장 상피세포 재생을 더 촉진시켰다. 이러한 결과들을 바탕으로, *A. muciniphila* 와 같은 뮤신 분해 균은 장 줄기세포가 연관된 장 상피세포 발달을 촉진하는데 중요한 역할을 하는 것으로 결론지을 수 있고, 더 나아가 장내 항상성 유지에 도움을 주는 것으로 사료 된다.

중심단어 : 장내 미생물, *Akkermansia muciniphila* (애커만시아 뮤시니필라), 장 줄기세포, 상피세포 발달